Please cite this document as: F. Stochino, G. Carta, SDOF models for reinforced concrete beams under impulsive loads accounting for strain rate effects, Nuclear Engineering and Design, Volume 276, September 2014, Pages 74-86, ISSN 0029-5493, http://dx.doi.org/10.1016/j.nucengdes.2014.05.022.

SDOF models for reinforced concrete beams under impulsive loads accounting for strain rate effects

Stochino F. [a] and Carta G. [b]

[a] Affiliation: Department of Civil and Environmental Engineering and Architecture, University of Cagliari

Address: Via Marengo 2, 09123 Cagliari, Italy

Telephone number: +39 070 675 5410

Fax number: +39 070 675 5418

E-mail address: fstochino@unica.it

[b] Corresponding author

Affiliation: Department of Mechanical, Chemical and Materials Engineering, University of Cagliari

Address: Via Marengo 2, 09123 Cagliari, Italy

Telephone number: +39 070 675 5410

Fax number: +39 070 675 5418

E-mail address: giorgio_carta@unica.it

Abstract

In this paper, reinforced concrete beams subjected to blast and impact loads are examined. Two single degree of freedom models are proposed to predict the response of the beam. The first model (denoted as "energy model") is developed from the law of energy balance and assumes that the deformed shape of the beam is represented by its first vibration mode. In the second model (named "dynamic model"), the dynamic behavior of the beam is simulated by a spring-mass oscillator. In both formulations, the strain rate dependencies of the constitutive properties of the beams are considered by varying the parameters of the models at each time step of the computation according to the values of the strain rates of the materials (i.e. concrete and reinforcing steels). The efficiency of each model is evaluated by comparing the theoretical results with experimental data found in literature. The comparison shows that the energy model gives a good estimation of the maximum deflection of the beam at collapse, defined as the attainment of the ultimate strain in concrete. On the other hand, the dynamic model generally provides a smaller value of the maximum

Please cite this document as: F. Stochino, G. Carta, SDOF models for reinforced concrete beams under impulsive loads accounting for strain rate effects, Nuclear Engineering and Design, Volume 276, September 2014, Pages 74-86, ISSN 0029-5493, http://dx.doi.org/10.1016/j.nucengdes.2014.05.022.

displacement. However, both approaches yield reliable results, even though they are based on some approximations. Being also very simple to implement, they may serve as an useful tool in practical applications.

Keywords: Blast loads; impact loads; RC beams; flexural failure; SDOF models; strain rate.

1. Introduction

Some special structures are designed in order to resist to exceptional events. For instance, military buildings or strategic constructions, such as nuclear power plants, may need to sustain blast loads caused by explosions; slabs and beams making up the structure of a turbine building or of an industrial warehouse can be subjected to the impacts of falling objects; retaining walls in mountainous regions are usually damaged by the falls of heavy rocks. Thus, the structural elements making up these special constructions should possess enough strength and ductility to withstand such dynamic loads without collapsing.

Explosions and impacts of falling objects represent two important cases of impulsive loads, which are characterized by rapid changes in time and by high intensity. Under these loads, structural elements experience very high strain rates, hence their constitutive properties do not remain constant but change significantly during time. Therefore, when analyzing the behavior of a structural element subjected to impulsive loads, it is necessary to account for the variations of material properties due to strain rates.

In practical applications, beams or columns acted upon by dynamic loads are usually schematized as Single Degree Of Freedom (SDOF) systems. Morison (2006) distinguished the SDOF methods in two groups: the Modal Method and the Equivalent SDOF Method. In the first, older approach, the response of the structural element is approximated by its first free vibration mode. In the second approach, instead, the beam (or the column) is modeled as a SDOF oscillator, the mass, resistance and load of which are related, respectively, to the kinetic energy, strain energy and external work of the represented beam. The Equivalent SDOF Method has proved to be the most efficient of the two approaches (Morison, 2006), so much so that it is still used nowadays. Different versions of the

Please cite this document as: F. Stochino, G. Carta, SDOF models for reinforced concrete beams under impulsive loads accounting for strain rate effects, Nuclear Engineering and Design, Volume 276, September 2014, Pages 74-86, ISSN 0029-5493, http://dx.doi.org/10.1016/j.nucengdes.2014.05.022.

Equivalent SDOF Method for the particular case of impulsive loads have been proposed so far. For example, Fisher and Häring (2009) determined the parameters of the SDOF system by minimizing the differences between the theoretical deflections and velocities provided by their model and the experimental responses given by blast tests. Yang and Lok (2007) derived the dynamic strength of a reinforced concrete structure from the analysis of a SDOF model, which includes strain rate effects. Nassr et al. (2013) used a SDOF model, which accounts both for secondary moment due to axial load and for the influence of strain rate, to investigate the strength and stability of steel columns subjected to blast loads.

In other, more sophisticated approaches, the beam is subdivided into many small elements along its length. These approaches, generally denoted as Multi Degree Of Freedom (MDOF) methods, allow to evaluate the overall response of the beam, and represent the basics of the finite elements (FE) codes. Li et al. (2009) developed a three-dimensional dynamic nonlinear FE model to study the response of a frame structure (typical of a turbine building) under explosions, focusing in particular on the effects of cladding panels. Fujikake et al. (2009) also considered the variation of strain rate effects along the depth of the beam cross-section by dividing the latter into fibers parallel to its width. Recently, Carta and Stochino (2013) have proposed a new method, whereby the equation of motion of a reinforced concrete beam is based on Euler-Bernoulli's theory and the elastic-plastic behavior of the beam is described by a smooth bending moment - curvature relationship. By solving the nonlinear equation of motion through a finite difference scheme, it is possible to calculate the response at any point of the beam axis and at any instant of time.

Numerical simulations based on the distinct element method have also been adopted. For instance, they were performed by Kusano et al. (1992) and by Masuya et al. (1994) to examine the behavior of concrete elements subjected to impact loads.

Structures under impulsive loads can be analyzed also by imposing energy balance conditions (Westine and Baker, 1975; Foo et al., 2011; Crupi et al., 2012). These "energy" models are usually simpler than MDOF approaches and require less computational effort. On the other hand, they

Please cite this document as: F. Stochino, G. Carta, SDOF models for reinforced concrete beams under impulsive loads accounting for strain rate effects, Nuclear Engineering and Design, Volume 276, September 2014, Pages 74-86, ISSN 0029-5493, http://dx.doi.org/10.1016/j.nucengdes.2014.05.022.
usually provide less details about the response of the structure.

The validity of any theoretical model needs to be assessed by comparing the results it provides with experimental data. For blast and impact loads, it is difficult to find thorough and accurate experimental works in literature. The reason is twofold: first, the experimental apparatus needed for the test is elaborate and expensive; second, national security laws rarely permit the circulation of information related to protection measures against bombs or other explosives. Two important exceptions are represented by the experimental works of Magnusson and Hallgren (2000, 2003, 2010), who tested many reinforced concrete beams to air blast loading, and of Fujikake et al. (2009), who subjected several under-reinforced concrete beams to the impacts of a drop hammer from different heights. Other experimental results for reinforced concrete members can be found in the papers by Hudson and Darwin (2005) and Tachibana et al. (2010). On the other hand, the behavior of steel elements under impulsive loads was investigated, for instance, by Alves and Jones (2002) and Nassr et al. (2012).

In this paper, reinforced concrete (RC) beams under blast and impact loads are examined. In particular, beams with low reinforcement ratio are considered, which generally fail in flexure. The properties of the materials and the characteristics of the cross-section of the beam are presented in Section 2. Two SDOF models are used to approximate the dynamic behavior of the beam, denoted as "energy model" and "dynamic model". They are thoroughly described in Section 3. For both approaches, strain rate effects are taken into account, as detailed in Section 4. In Section 5, the theoretical results given by the two models are compared with the experimental findings carried out by Magnusson and Hallgren (2000) for the case of blast loads, while the tests performed by Fujikake et al. (2009) are used as benchmark for the case of impact loads. The effects of strain rate are shown explicitly in Section 6. Finally, some concluding remarks are provided in Section 7.

2. Material and sectional properties of the beam

2.1 Constitutive properties of concrete and reinforcing steel

The stress-strain relations of concrete and reinforcing steel are drawn from the *fib Bulletin n. 55*

Please cite this document as: F. Stochino, G. Carta, SDOF models for reinforced concrete beams under impulsive loads accounting for strain rate effects, Nuclear Engineering and Design, Volume 276, September 2014, Pages 74-86, ISSN 0029-5493, http://dx.doi.org/10.1016/j.nucengdes.2014.05.022.
(2010), and they are reported in the following.

In case of uniaxial compression, concrete stress σ_c (<0) and strain ε_c (<0) are related by the following expression (fib, 2010, § 5.1.8.1):

$$\sigma_c = f_{cm}\frac{k\cdot\varepsilon_c/\varepsilon_{c1}-(\varepsilon_c/\varepsilon_{c1})^2}{1+(k-2)\cdot\varepsilon_c/\varepsilon_{c1}} \quad \text{for } |\varepsilon_c| < |\varepsilon_{c,lim}|, \tag{1}$$

where the quantities f_{cm}, k, ε_{c1} and $\varepsilon_{c,lim}$ depend on the concrete grade (fib, 2010, Table 5.1-8). Eq. (1) is plotted qualitatively in Fig. 1a, where f_{cu} is the ultimate compressive strength of concrete. The tensile strength of concrete is neglected, since it is significantly lower than its compressive strength.

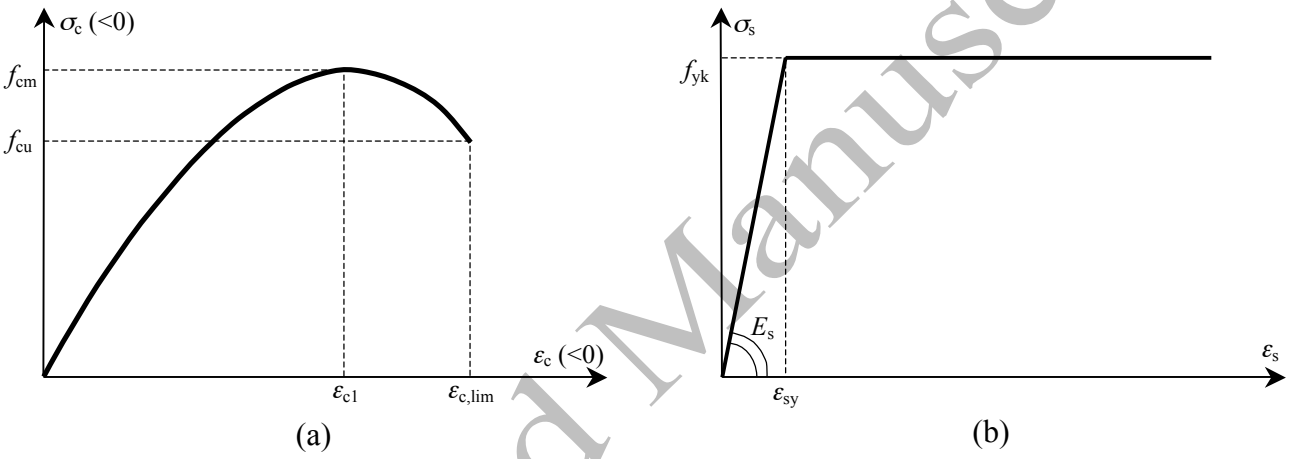

Fig. 1: Relations between stress and strain for concrete (a) and reinforcing steel (b) considered in this paper.

The elastic-plastic behavior of reinforcing steel can be idealized by the bilinear diagram sketched in Fig. 1b (fib, 2010, § 5.2.9). The quantities E_s, f_{yk} and ε_{sy} shown in Fig. 1b represent, respectively, the Young's modulus, the yield strength and the yield strain of steel. The stress-strain diagram of reinforcing steel is assumed to be symmetrical in tension and compression.

2.2 Characteristic properties of the cross-section at the yield and ultimate states

In this work, the yield state is defined as the attainment of the yield stress in the tensile reinforcement, i.e. $\sigma_s = f_{yk}$. On the other hand, it is assumed that the ultimate state (or collapse) is achieved when concrete reaches its maximum compressive strain, i.e. $\varepsilon_c = \varepsilon_{c,lim}$.

For a doubly reinforced concrete beam, the cross-section of which is shown in Fig. 2a, the stress

Please cite this document as: F. Stochino, G. Carta, SDOF models for reinforced concrete beams under impulsive loads accounting for strain rate effects, Nuclear Engineering and Design, Volume 276, September 2014, Pages 74-86, ISSN 0029-5493, http://dx.doi.org/10.1016/j.nucengdes.2014.05.022.

and strain diagrams at the yield state are plotted in Figs. 2b and 2c, respectively. The neutral axis depth at the yield state, here indicated by x_y, is calculated from the translational equilibrium condition, given by

$$b\int_0^{x_y}\sigma_c\,dy+\sigma_{ss}A_{ss}=f_{yk}A_s. \tag{2}$$

In the equation above, b is the width of the cross-section, σ_{ss} is the stress in the compressive reinforcement, while A_s and A_{ss} are the areas of tensile and compressive reinforcements.[1] By using Eq. (1) and the strain diagram at the yield state shown in Fig. 2c, Eq. (2) becomes

$$b f_{cm}\int_0^{x_y}\left[\frac{k\frac{\varepsilon_{sy}}{\varepsilon_{c1}}\frac{x_y-y}{d-x_y}-\left(\frac{\varepsilon_{sy}}{\varepsilon_{c1}}\frac{x_y-y}{d-x_y}\right)^2}{1+(k-2)\frac{\varepsilon_{sy}}{\varepsilon_{c1}}\frac{x_y-y}{d-x_y}}\right]dy+E_s\,\varepsilon_{sy}\frac{x_y-d'}{d-x_y}A_{ss}=f_{yk}A_s \quad \text{if } \varepsilon_{ss}<\varepsilon_{sy}; \tag{3a}$$

$$b f_{cm}\int_0^{x_y}\left[\frac{k\frac{\varepsilon_{sy}}{\varepsilon_{c1}}\frac{x_y-y}{d-x_y}-\left(\frac{\varepsilon_{sy}}{\varepsilon_{c1}}\frac{x_y-y}{d-x_y}\right)^2}{1+(k-2)\frac{\varepsilon_{sy}}{\varepsilon_{c1}}\frac{x_y-y}{d-x_y}}\right]dy+f_{yk}A_{ss}=f_{yk}A_s \quad \text{if } \varepsilon_{ss}\geq\varepsilon_{sy}. \tag{3b}$$

In the formulae above, d and d' stand for the effective depths of tensile and compressive reinforcements, respectively.

The resistant bending moment at the yield state, here denoted by M_y, can be obtained by imposing the equilibrium of rotation around the tensile reinforcement:

$$M_y=b\int_0^{x_y}\sigma_c(d-y)\,dy+\sigma_{ss}A_{ss}(d-d'). \tag{4}$$

By introducing the expression (2) of σ_c into Eq. (4) and assuming a linear strain distribution, the expression of M_y is modified as follows:

[1] In this paper, the subscripts "s" and "ss" are used to distinguish quantities related to tensile and compressive reinforcements, respectively.

Please cite this document as: F. Stochino, G. Carta, SDOF models for reinforced concrete beams under impulsive loads accounting for strain rate effects, Nuclear Engineering and Design, Volume 276, September 2014, Pages 74-86, ISSN 0029-5493, http://dx.doi.org/10.1016/j.nucengdes.2014.05.022.

$$M_y = b f_{cm} \int_0^{x_y} \left[\frac{k \frac{\varepsilon_{sy}}{\varepsilon_{c1}} \frac{x_y - y}{d - x_y} - \left(\frac{\varepsilon_{sy}}{\varepsilon_{c1}} \frac{x_y - y}{d - x_y} \right)^2}{1 + (k-2) \frac{\varepsilon_{sy}}{\varepsilon_{c1}} \frac{x_y - y}{d - x_y}} \right] (d - y)\,\mathrm{d}y + E_s \varepsilon_{sy} \frac{x_y - d'}{d - x_y} A_{ss} (d - d') \quad \text{if } \varepsilon_{ss} < \varepsilon_{sy}; \tag{5a}$$

$$M_y = b f_{cm} \int_0^{x_y} \left[\frac{k \frac{\varepsilon_{sy}}{\varepsilon_{c1}} \frac{x_y - y}{d - x_y} - \left(\frac{\varepsilon_{sy}}{\varepsilon_{c1}} \frac{x_y - y}{d - x_y} \right)^2}{1 + (k-2) \frac{\varepsilon_{sy}}{\varepsilon_{c1}} \frac{x_y - y}{d - x_y}} \right] (d - y)\,\mathrm{d}y + f_{yk} A_{ss} (d - d') \quad \text{if } \varepsilon_{ss} \geq \varepsilon_{sy}. \tag{5b}$$

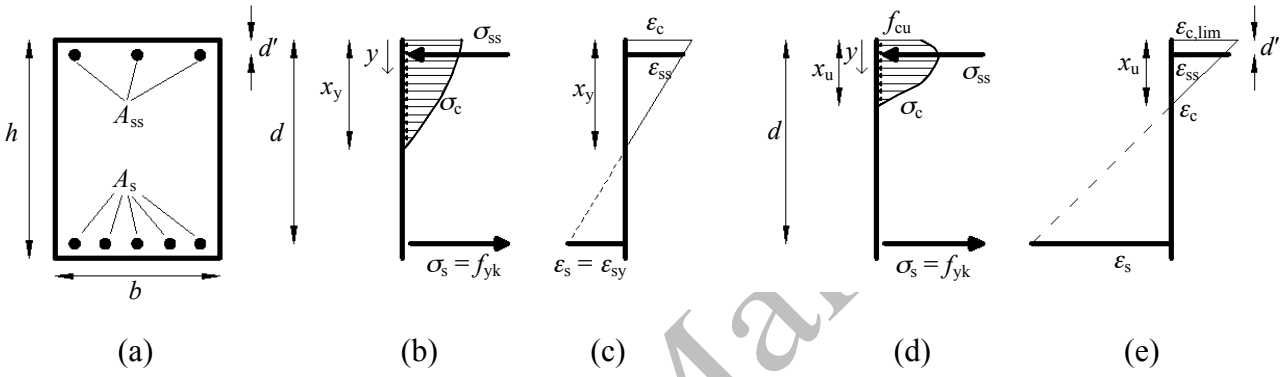

Fig. 2: (a) Cross-section of a doubly reinforced concrete beam. Yield state: stress diagram (b) and strain diagram (c). Ultimate state: stress diagram (d) and strain diagram (e).

The stress and strain diagrams at the ultimate state are represented schematically in Figs. 2d and 2e, respectively. The neutral axis depth x_u and the resistant bending moment M_u are determined from the translational and rotational equations of equilibrium at the ultimate state, respectively. In particular, x_u is obtained by solving either of the following implicit equations:

$$b f_{cm} \int_0^{x_u} \left[\frac{k \frac{\varepsilon_{c,lim}}{\varepsilon_{c1}} \frac{x_u - y}{x_u} - \left(\frac{\varepsilon_{c,lim}}{\varepsilon_{c1}} \frac{x_u - y}{x_u} \right)^2}{1 + (k-2) \frac{\varepsilon_{c,lim}}{\varepsilon_{c1}} \frac{x_u - y}{x_u}} \right] \mathrm{d}y + E_s \varepsilon_{c,lim} \frac{x_u - d'}{x_u} A_{ss} = f_{yk} A_s \quad \text{if } \varepsilon_{ss} < \varepsilon_{sy}; \tag{6a}$$

$$b f_{cm} \int_0^{x_u} \left[\frac{k \frac{\varepsilon_{c,lim}}{\varepsilon_{c1}} \frac{x_u - y}{x_u} - \left(\frac{\varepsilon_{c,lim}}{\varepsilon_{c1}} \frac{x_u - y}{x_u} \right)^2}{1 + (k-2) \frac{\varepsilon_{c,lim}}{\varepsilon_{c1}} \frac{x_u - y}{x_u}} \right] \mathrm{d}y + f_{yk} A_{ss} = f_{yk} A_s \quad \text{if } \varepsilon_{ss} \geq \varepsilon_{sy}. \tag{6b}$$

Please cite this document as: F. Stochino, G. Carta, SDOF models for reinforced concrete beams under impulsive loads accounting for strain rate effects, Nuclear Engineering and Design, Volume 276, September 2014, Pages 74-86, ISSN 0029-5493, http://dx.doi.org/10.1016/j.nucengdes.2014.05.022.

M_u is given explicitly by either of the following expressions:

$$M_u = b f_{cm} \int_0^{x_u} \left[\frac{k \frac{\varepsilon_{c,lim}}{\varepsilon_{c1}} \frac{x_u - y}{x_u} - \left(\frac{\varepsilon_{c,lim}}{\varepsilon_{c1}} \frac{x_u - y}{x_u} \right)^2}{1 + (k-2) \frac{\varepsilon_{c,lim}}{\varepsilon_{c1}} \frac{x_u - y}{x_u}} \right] (d - y) \, dy + E_s \, \varepsilon_{c,lim} \frac{x_u - d'}{x_u} A_{ss} (d - d') \quad \text{if } \varepsilon_{ss} < \varepsilon_{sy}; \quad (7a)$$

$$M_u = b f_{cm} \int_0^{x_u} \left[\frac{k \frac{\varepsilon_{c,lim}}{\varepsilon_{c1}} \frac{x_u - y}{x_u} - \left(\frac{\varepsilon_{c,lim}}{\varepsilon_{c1}} \frac{x_u - y}{x_u} \right)^2}{1 + (k-2) \frac{\varepsilon_{c,lim}}{\varepsilon_{c1}} \frac{x_u - y}{x_u}} \right] (d - y) \, dy + f_{yk} \, A_{ss} (d - d') \quad \text{if } \varepsilon_{ss} \geq \varepsilon_{sy}. \quad (7b)$$

Finally, the curvature at the yield state θ_y is given by

$$\theta_y = \frac{\varepsilon_{sy}}{d - x_y}, \quad (8)$$

while the curvature at the ultimate state θ_u is calculated with the following formula:

$$\theta_u = \frac{\varepsilon_{c,lim}}{x_u}. \quad (9)$$

2.3 Bending moment - curvature relation

The relation between bending moment M and curvature θ is usually approximated by a bilinear diagram[2], which is obtained by using the quantities θ_y, θ_u, M_y and M_u, determined in Section 2.2. This diagram (which is shown in Fig. 3a) allows to simplify the formulation of the problem and the calculations. However, it does not provide a satisfactory representation of the physical reality. In fact, experimental flexural tests on reinforced concrete beams rarely show an abrupt transition from the elastic to the plastic regime.

A smoother relationship between bending moment and curvature in the whole deformation range is adopted in this paper (see also Carta and Stochino, 2013), which reads

$$M = \bar{M} \tanh\left(\frac{\bar{K}}{\bar{M}} \theta \right). \quad (10)$$

[2] In other approaches a trilinear diagram is considered, in which the first change of slope coincides with the first cracking of concrete. In this work this situation is not taken into account, because the tensile strength of concrete is disregarded.

Please cite this document as: F. Stochino, G. Carta, SDOF models for reinforced concrete beams under impulsive loads accounting for strain rate effects, Nuclear Engineering and Design, Volume 276, September 2014, Pages 74-86, ISSN 0029-5493, http://dx.doi.org/10.1016/j.nucengdes.2014.05.022.

The relation (10), which is plotted in Fig. 3b, has proved to give better results than the bilinear diagram of Fig. 3a (Carta and Stochino, 2013). The parameters $\bar{K}$ and $\bar{M}$ represent, respectively, the initial slope of the curve and the maximum value of the bending moment. They can be estimated from the bilinear diagram of Fig. 3a. In particular, $\bar{K}$ is taken as

$$\bar{K} = \frac{M_y}{\theta_y}. \tag{11}$$

$\bar{M}$ is calculated by assuming that the areas A_1 and A_2, shown in Figs. 3a and 3b, are equal. The equivalence of A_1 and A_2, based on energy considerations, leads to the following implicit equation:

$$A_1 = A_2 \quad \Rightarrow \quad \frac{M_u\left(\theta_u - \theta_y\right) + M_y\theta_u}{2} = \frac{\bar{M}^2}{\bar{K}} \ln\left[\cosh\left(\frac{\bar{K}}{\bar{M}}\theta_u\right)\right], \tag{12}$$

from which $\bar{M}$ can be derived.

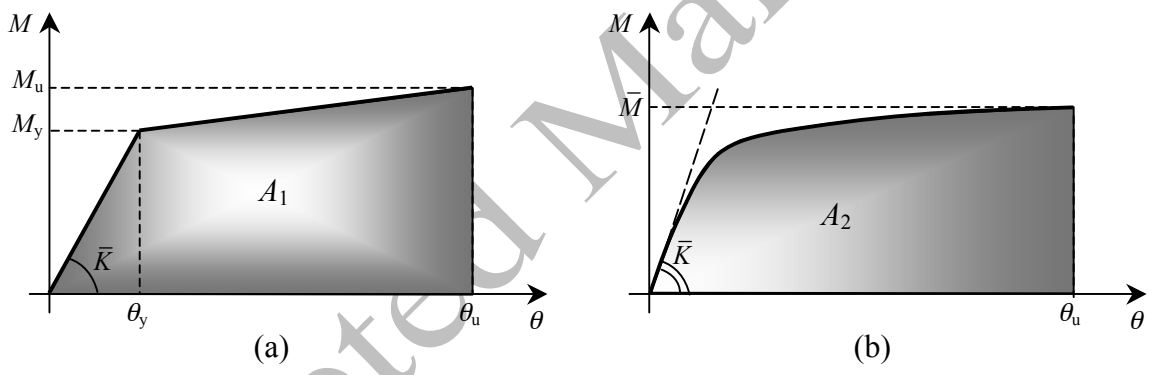

Fig. 3: (a) Bilinear relation between bending moment and curvature; (b) smooth bending moment - curvature relation considered in this work, obtained from Eq. (10).

3. Description of the SDOF models

In this section, two SDOF models are described. The first one is based on energy balance, therefore it will be referred to as "energy model". The second one, instead, is denoted as "dynamic model", because it is developed from the equation of motion of a SDOF oscillator, which simulates the dynamic behavior of the beam.

Damping is not considered in this paper, because the maximum displacement is obtained in the first cycle of loading. In fact, the aim of this paper is to evaluate the displacement of the beam at

Please cite this document as: F. Stochino, G. Carta, SDOF models for reinforced concrete beams under impulsive loads accounting for strain rate effects, Nuclear Engineering and Design, Volume 276, September 2014, Pages 74-86, ISSN 0029-5493, http://dx.doi.org/10.1016/j.nucengdes.2014.05.022.

collapse, which is generally achieved during the loading process (Riedel et al., 2012). Moreover, since the time when the impulsive load is applied is generally much smaller than the oscillation period of the beam, the failure of the beam usually occurs before the first peak of oscillation.

3.1 Energy model

The conservation of energy law requires that the external work on the beam (W) equal the sum of the kinetic energy (K) and the strain energy (U) of the beam at each instant of time:

$$W(t) = K(t) + U(t)\,. \tag{13}$$

The external work is given by

$$W(t) = \int_0^t \int_0^l q(x,t)\frac{\partial v(x,t)}{\partial t}\,\mathrm{d}x\,\mathrm{d}t + \int_0^t \sum_{i=1}^{n} F_i(t)\frac{\partial v(x_i,t)}{\partial t}\,\mathrm{d}t + \int_0^t \sum_{j=1}^{m} M_j(t)\frac{\partial}{\partial t}\left[\frac{\partial v}{\partial x}(x_j,t)\right]\mathrm{d}t\,, \tag{14}$$

where x is the axial coordinate, t is time, l is the length of the beam, v is the transverse displacement, q is the transverse distributed load, F_i are the point forces (perpendicular to x) and M_j are the concentrated moments, as shown in Fig. 4.

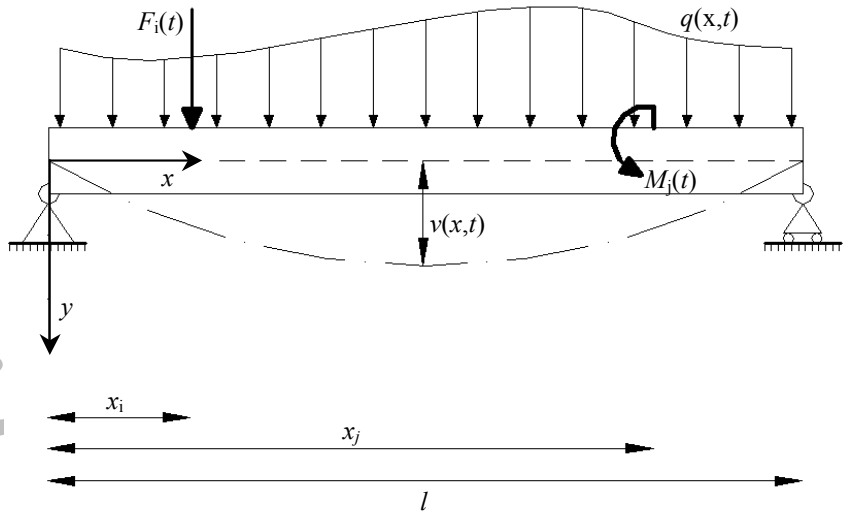

Fig. 4: Schematic representation of the beam, subjected to a distributed load q, to point forces F_i and to concentrated moments M_j.

The kinetic energy of the beam can be written as

Please cite this document as: F. Stochino, G. Carta, SDOF models for reinforced concrete beams under impulsive loads accounting for strain rate effects, Nuclear Engineering and Design, Volume 276, September 2014, Pages 74-86, ISSN 0029-5493, http://dx.doi.org/10.1016/j.nucengdes.2014.05.022.

$$K(t) = \int_0^l \frac{1}{2}\mu\left[\frac{\partial v(x,t)}{\partial t}\right]^2 \mathrm{d}x, \tag{15}$$

where μ is the mass per unit length.

By using Eq. (10) to relate bending moment and curvature and neglecting axial and shear deformations (which are much smaller than flexural deformations), the strain energy of the beam is defined as

$$U(t) = \int_0^l \int_0^{\theta(x,t)} \bar{M}\tanh\left[\frac{\bar{K}}{\bar{M}}\theta(x,t)\right]\mathrm{d}\theta\,\mathrm{d}x = \int_0^l \frac{\bar{M}^2}{\bar{K}}\ln\left\{\cosh\left[-\frac{\bar{K}}{\bar{M}}\frac{\partial^2 v(x,t)}{\partial x^2}\right]\right\}\mathrm{d}x; \tag{16}$$

where $\theta = -\partial^2 v/\partial x^2$ in the chosen reference system (see Fig. 4).

For a simply supported beam under symmetrical loads, as will be considered in Section 5, the deformed shape of the beam $v(x,t)$ can be expressed as the sum of odd sinusoidal modes:

$$v(x,t) = \sum_{i=1,3,5,\ldots}^{\infty} V_i(t)\sin\left(\frac{i\pi x}{l}\right). \tag{17}$$

Cox et al. (1978) proved that the difference between the maximum strain obtained by taking only the first mode ($i = 1$) and the maximum strain determined by accounting also for the third mode ($i = 3$) is less than 3%. Therefore, in the present work it is assumed that the displacement function is given by

$$v(x,t) = V_0(t)\sin\left(\frac{\pi x}{l}\right), \tag{18}$$

which contains the only unknown $V_0(t)$. Accordingly, the curvature is expressed by

$$\theta(x,t) = -\frac{\partial^2 v(x,t)}{\partial x^2} = \frac{\pi^2}{l^2}V_0(t)\sin\left(\frac{\pi x}{l}\right). \tag{19}$$

With this approximation, the kinetic and strain energy of the beam assume the following forms:

$$K(t) = \int_0^l \frac{1}{2}\mu\left[\frac{\partial V_0(t)}{\partial t}\right]^2 \sin^2\left(\frac{\pi x}{l}\right)\mathrm{d}x = \frac{\mu l}{4}\left[\frac{\partial V_0(t)}{\partial t}\right]^2; \tag{20}$$

$$U(t) = \int_0^l \frac{\bar{M}^2}{\bar{K}}\ln\left\{\cosh\left[\frac{\bar{K}}{\bar{M}}\frac{\pi^2}{l^2}V_0(t)\sin\left(\frac{\pi x}{l}\right)\right]\right\}\mathrm{d}x. \tag{21}$$

Please cite this document as: F. Stochino, G. Carta, SDOF models for reinforced concrete beams under impulsive loads accounting for strain rate effects, Nuclear Engineering and Design, Volume 276, September 2014, Pages 74-86, ISSN 0029-5493, http://dx.doi.org/10.1016/j.nucengdes.2014.05.022.

The external work depends on the loads acting on the beam. In Section 5 two kinds of external loads are examined: a uniformly distributed load $q_0(t)$, and a point force $F(t)$ applied at the mid-span section of the beam. For these two cases, the external work is given by

$$W(t) = \int_0^t \int_0^l q_0(t) \frac{\partial V_0(t)}{\partial t} \sin\left(\frac{\pi x}{l}\right) \mathrm{d}x \, \mathrm{d}t = \int_0^t \frac{2l}{\pi} q_0(t) \frac{\partial V_0(t)}{\partial t} \mathrm{d}t \tag{22a}$$

and

$$W(t) = \int_0^t F(t) \frac{\partial V_0(t)}{\partial t} \mathrm{d}t \,, \tag{22b}$$

respectively.

After substituting Eq. (20), Eq. (21) and either Eq. (22a) or Eq. (22b) into Eq. (13), the latter is solved in Section 5 by employing the Finite Difference approach. The integral appearing in Eq. (21) is computed numerically through the trapezoidal method.

3.2 Dynamic model

The dynamic study of the beam can be performed by idealizing the beam as a SDOF oscillator (see Fig. 5a), consisting of a lumped mass and an elastic spring.

The properties of the equivalent SDOF oscillator are labeled with the subscript "E". In particular, M_E denotes the equivalent mass of the oscillator, which is given by $M_E = K_{LM} \cdot M_b$, where M_b is the mass of the beam and K_{LM} is a coefficient which accounts for the boundary conditions of the beam, the type of load and the regime considered (elastic or plastic). For example, for a simply supported beam, $M_{E,el} = 0.78 \cdot M_b$ and $M_{E,pl} = 0.66 \cdot M_b$ in case of a uniformly distributed load, while $M_{E,el} = 0.49 \cdot M_b$ and $M_{E,pl} = 0.33 \cdot M_b$ in case of a point force applied at the mid-span section of the beam (Biggs, 1964, Table 5.1). On the other hand, v_E represents the displacement of the equivalent SDOF oscillator corresponding to the mid-span deflection of the beam, while P_E is the load acting on it. The latter is taken as $P_E(t) = q_0(t) \cdot l$ (if the beam is subjected to a uniformly distributed load q_0) or as $P_E(t) = F(t)$ (when the beam is excited by a point force F at the middle point of its axis). Finally, K_E is the equivalent stiffness, which varies from the elastic to the plastic range, as shown in the

Please cite this document as: F. Stochino, G. Carta, SDOF models for reinforced concrete beams under impulsive loads accounting for strain rate effects, Nuclear Engineering and Design, Volume 276, September 2014, Pages 74-86, ISSN 0029-5493, http://dx.doi.org/10.1016/j.nucengdes.2014.05.022.
following.

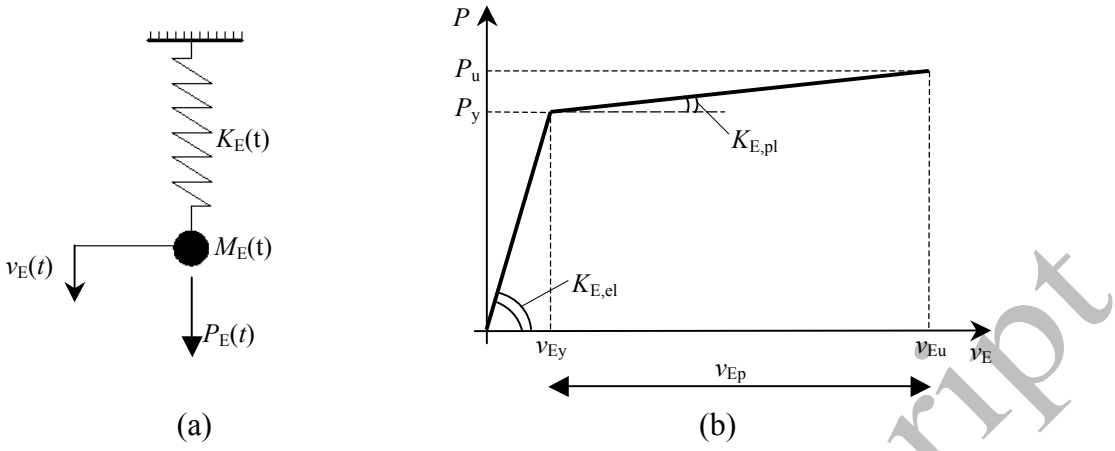

Fig. 5: (a) Equivalent SDOF oscillator representing the beam of Fig. 4, having mass M_E and stiffness K_E; the displacement generated by the force P_E is indicated by v_E. (b) Load-displacement diagram of the equivalent SDOF oscillator.

The SDOF oscillator is assumed to be characterized by a bilinear load - displacement diagram, as sketched in Fig. 5b. The yield load P_y and the ultimate load P_u are obtained from equilibrium conditions. In particular, for the case of a uniformly distributed transverse load, they are given by

$$P_y = \frac{8 \cdot M_y}{l}; \tag{23a}$$

$$P_u = \frac{8 \cdot M_u}{l}. \tag{23b}$$

On the other hand, when the beam is loaded by a transverse point force applied at its mid-span section, P_y and P_u are calculated as

$$P_y = \frac{4 \cdot M_y}{l}; \tag{24a}$$

$$P_u = \frac{4 \cdot M_u}{l}. \tag{24b}$$

The yield displacement v_{Ey} is determined from the elastic theory of structures. More specifically, for a uniformly distributed load:

Please cite this document as: F. Stochino, G. Carta, SDOF models for reinforced concrete beams under impulsive loads accounting for strain rate effects, Nuclear Engineering and Design, Volume 276, September 2014, Pages 74-86, ISSN 0029-5493, http://dx.doi.org/10.1016/j.nucengdes.2014.05.022.

$$v_{Ey} = \frac{5 P_y l^3}{384 \bar{K}}, \tag{25a}$$

while for a point force applied at the center of the beam axis:

$$v_{Ey} = \frac{P_y l^3}{48 \bar{K}}. \tag{25b}$$

In the formulae above, $\bar{K}$ is the flexural stiffness of the beam, given by Eq. (11). When deriving Eqs. (23) and Eq. (25a), it was assumed that $P_y = q_y \cdot l$ and $P_u = q_u \cdot l$, where q_y and q_u are the values of the uniformly distributed load at the yield and ultimate states, respectively. The last quantity that needs to be determined in order to construct the load - displacement diagram of the SDOF oscillator is v_{Eu}, which represents the ultimate displacement of the SDOF oscillator. Its plastic component v_{Ep} can be evaluated assuming the formation of a plastic hinge, as shown in Fig. 6. In this scenario, v_{Eu} can be expressed by

$$v_{Eu} = v_{Ey} + v_{Ep} = v_{Ey} + \frac{\varphi_p}{2} \cdot \frac{l}{2} = v_{Ey} + \frac{\theta_p \cdot l_p}{2} \cdot \frac{l}{2} = v_{Ey} + \frac{1}{4} \cdot (\theta_u - \theta_y) \cdot l_p \cdot l. \tag{26}$$

In the equation above, φ_p is the plastic rotation, l_p is the length of the plastic hinge and $\theta_p = \theta_u - \theta_y$ is the plastic curvature. The length of the plastic hinge cannot be calculated exactly. In this work, it is estimated by the following approximate formula proposed by Mattock (see Fujikake et al., 2009):

$$l_p = d + 0.05 \cdot l. \tag{27}$$

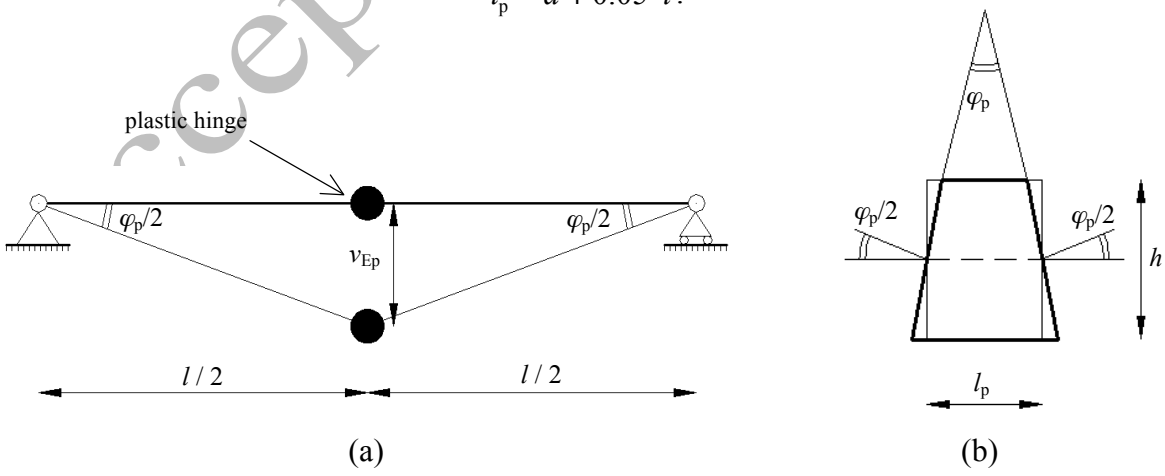

Fig. 6: (a) Assumed deformation mechanism in the plastic range, with the generation of a plastic hinge at the mid-span section of the beam; (b) detail of the plastic hinge.

Please cite this document as: F. Stochino, G. Carta, SDOF models for reinforced concrete beams under impulsive loads accounting for strain rate effects, Nuclear Engineering and Design, Volume 276, September 2014, Pages 74-86, ISSN 0029-5493, http://dx.doi.org/10.1016/j.nucengdes.2014.05.022.

The equivalent stiffnesses in the elastic range ($K_{E,el}$) and in the plastic range ($K_{E,pl}$) can be obtained from simple geometric calculations (refer to Fig. 5b):

$$K_{E,el} = \frac{P_y}{v_{Ey}}; \tag{28a}$$

$$K_{E,pl} = \frac{P_u - P_y}{v_{Eu} - v_{Ey}}. \tag{28b}$$

Finally, the equations of motion of the equivalent SDOF oscillator in the elastic and plastic regimes have the following forms:

$$M_{E,el}\frac{d^2 v_E(t)}{dt^2} + K_{E,el}(t)\,v_E(t) = P_E(t) \quad \text{for } 0 \le v_E \le v_{Ey}; \tag{29a}$$

$$M_{E,pl}\frac{d^2 v_E(t)}{dt^2} + K_{E,pl}(t)\,v_E(t) + \left[K_{E,el}(t) - K_{E,pl}(t)\right] v_{Ey} = P_E(t) \quad \text{for } v_{Ey} < v_E \le v_{Eu}. \tag{29b}$$

The ordinary differential equations (29) are integrated in Section 5 by employing the Finite Difference method.

4. Introduction of strain rate sensitivity into the formulations of the SDOF models

4.1 Dependence of material properties on strain rate

The constitutive properties of concrete and reinforcing steel vary significantly with strain rate. The strain rate dependence of each property of both materials is specified by the *CEB Information Bulletin n. 187* (1988), as reported below. The superscript "dyn" (which is the abbreviation for "dynamic") will be henceforth appended to the quantities that are modified by strain rate.

The dynamic strength of concrete is calculated with either of the following formulae (CEB, 1988, § 3.3.1):

$$f_{cm}^{dyn} = f_{cm} \cdot \left(\frac{\dot{\varepsilon}_c}{30 \cdot 10^{-6}}\right)^{1.026\cdot\alpha} \quad \text{if } \dot{\varepsilon}_c \le 30\,\text{s}^{-1}; \tag{30a}$$

$$f_{cm}^{dyn} = f_{cm} \cdot \gamma \cdot \dot{\varepsilon}_c^{1/3} \quad \text{if } \dot{\varepsilon}_c > 30\,\text{s}^{-1}. \tag{30b}$$

Please cite this document as: F. Stochino, G. Carta, SDOF models for reinforced concrete beams under impulsive loads accounting for strain rate effects, Nuclear Engineering and Design, Volume 276, September 2014, Pages 74-86, ISSN 0029-5493, http://dx.doi.org/10.1016/j.nucengdes.2014.05.022.

Here $\dot{\varepsilon}_c$ represents the strain rate of concrete, while α and γ are two parameters given by $\alpha = 1/(5+3\cdot f_{cm}/4)$ and $\gamma = 10\text{^}(6.156\cdot\alpha\text{-}0.492)$, respectively. The static concrete strains ε_{c1} and $\varepsilon_{c,lim}$ are increased by using the following expressions (CEB, 1988, § 3.3.1; Asprone et al., 2012):

$$\varepsilon_{c1}^{dyn} = \varepsilon_{c1} \cdot \left(\frac{\dot{\varepsilon}_c}{30 \cdot 10^{-6}} \right)^{0.02}; \tag{31a}$$

$$\varepsilon_{c,lim}^{dyn} = \varepsilon_{c,lim} \cdot \left(\frac{\dot{\varepsilon}_c}{30 \cdot 10^{-6}} \right)^{0.02}. \tag{31b}$$

The dynamic strength of reinforcing steel (both in tension and in compression) is augmented by the strain rate $\dot{\varepsilon}^s$ according to either of the following relations (CEB, 1988, § 3.4.2):

$$f_{yk}^{dyn} = f_{yk} \cdot \left[1 + \frac{6}{f_{yk}} \ln\left(\frac{\dot{\varepsilon}^s}{5 \cdot 10^{-5}} \right) \right] \quad \text{if } \dot{\varepsilon}^s \le 10\,\text{s}^{-1}; \tag{32a}$$

$$f_{yk}^{dyn} = f_{yk} \cdot \left[1 + \frac{6}{f_{yk}} \ln\left(2 \cdot 10^{5} \right) \right] \quad \text{if } \dot{\varepsilon}^s > 10\,\text{s}^{-1}. \tag{32b}$$

On the other hand, the Young's modulus E_s does not depend on strain rate (CEB, 1988, § 3.4.3).

4.2 Procedure to account for strain rate in the energy model

The properties of both concrete and steel are modified at each time step of the computation by using Eqs. (30)-(32). Since the constitutive properties of the two materials depend on their strain rates, the latter need to be calculated. Thus, after deriving the initial sectional characteristics (x_y, M_y, x_u, M_u, $\bar{K}$, $\bar{M}$) from the static material properties, the following procedure is carried out at each time step:

1) the transverse displacement V_0 appearing in Eq. (18) is determined by solving Eq. (13), as outlined at the end of Section 3.1;

2) the maximum curvature $\theta = \pi^2/l^2 \cdot V_0$ (see Eq. (19)) is calculated;

3) considering the value of the curvature at the previous instant of time,

the rate of curvature $\dot{\theta} = \partial\theta/\partial t$ is obtained;

4) the bending moment M corresponding to the curvature θ is found from Eq. (10);

Please cite this document as: F. Stochino, G. Carta, SDOF models for reinforced concrete beams under impulsive loads accounting for strain rate effects, Nuclear Engineering and Design, Volume 276, September 2014, Pages 74-86, ISSN 0029-5493, http://dx.doi.org/10.1016/j.nucengdes.2014.05.022.

5) the value of M is used to calculate the neutral axis depth x by means of the rotational equilibrium equation around the tensile reinforcement;

6) the strain of concrete and the strains of tensile and compressive reinforcements are obtained by using the linear strain diagram (which can be easily constructed knowing the values of x and θ): $\varepsilon_c = \theta \cdot x$, $\varepsilon_s = \theta \cdot (d-x)$, $\varepsilon_{ss} = \theta \cdot (x-d')$;

7) by referring to the values of the strains at the previous time step, the rates of strain of concrete and steel reinforcements are determined;

8) the augmented properties of the material are evaluated according to Eqs. (30)-(32);

9) the values of the sectional characteristics (x_y, M_y, x_u, M_u) are updated;

10) the new values of $\bar{K}$ and $\bar{M}$ are calculated from Eqs. (11) and (12).

This procedure is stopped when concrete reaches its ultimate strain, i.e. when the criterion of collapse is fulfilled.

4.3 Procedure to account for strain rate in the dynamic model

The procedure to include the effects of strain rate into the formulation of the dynamic model is very similar to that relative to the energy model, described in the previous section. Only the first three steps are different:

1) at each time step, the equivalent displacement of the SDOF oscillator v_E is calculated from either Eq. (29a) or Eq. (29b), for instance by using the Finite Difference approach;

2) the equivalent velocity $\dot{v}_E = \mathrm{d}v_E / \mathrm{d}t$ is obtained by knowing the value of v_E at the previous time step;

3) the equivalent curvature θ_E and its rate $\dot{\theta}_E$ can be assessed by linking the SDOF oscillator to the beam it represents. For clarity's sake, the case of a simply supported beam is examined in the following. In the elastic regime, θ_E and $\dot{\theta}_E$ can be easily obtained from the elastic theory of structures. In particular, if a uniformly distributed load is imposed, they are given by the following expressions:

Please cite this document as: F. Stochino, G. Carta, SDOF models for reinforced concrete beams under impulsive loads accounting for strain rate effects, Nuclear Engineering and Design, Volume 276, September 2014, Pages 74-86, ISSN 0029-5493, http://dx.doi.org/10.1016/j.nucengdes.2014.05.022.

$$\theta_E = \frac{48 \cdot v_E}{5 \cdot l^2} \quad \text{for } 0 \le v_E \le v_{Ey}; \tag{33a}$$

$$\dot{\theta}_E = \frac{48 \cdot \dot{v}_E}{5 \cdot l^2} \quad \text{for } 0 \le v_E \le v_{Ey}. \tag{33b}$$

On the other hand, if the beam is subjected to a point force at its mid-span section, they are calculated through the following formulae:

$$\theta_E = \frac{12 \cdot v_E}{l^2} \quad \text{for } 0 \le v_E \le v_{Ey}; \tag{34a}$$

$$\dot{\theta}_E = \frac{12 \cdot \dot{v}_E}{l^2} \quad \text{for } 0 \le v_E \le v_{Ey}. \tag{34b}$$

In the plastic regime, θ_E and $\dot{\theta}_E$ are instead evaluated by referring to the deformation mechanism of Fig. 6. Simple geometric considerations yield:

$$\theta_E = \theta_y + \frac{\varphi_p}{l_p} = \theta_y + 2 \cdot \frac{v_E - v_{Ey}}{l/2} \cdot \frac{1}{l_p} \quad \text{for } v_{Ey} \le v_E \le v_{Eu}; \tag{35a}$$

$$\dot{\theta}_E = 2 \cdot \frac{\dot{v}_E}{l/2} \cdot \frac{1}{l_p} \quad \text{for } v_{Ey} \le v_E \le v_{Eu}. \tag{35b}$$

Here, v_E - v_{Ey} represents the plastic displacement.

The computational process continues by following the steps 4-10 described in Section 4.2.

5. Comparison with experimental data

In this section, the validity of each SDOF model proposed in this work is verified through comparison with some experimental data available in literature. Two different situations are investigated. In the first case, a simply supported beam subjected to a uniformly distributed load produced by an explosion is examined. The second setup consists of a simply supported beam under a point force at its mid-span section, caused by the impact of a drop hammer.

5.1 RC beam under explosion

In this application, the experimental findings presented in a report by Magnusson and Hallgren (2000) are taken as benchmark. These two authors carried out a series of tests, in which they

Please cite this document as: F. Stochino, G. Carta, SDOF models for reinforced concrete beams under impulsive loads accounting for strain rate effects, Nuclear Engineering and Design, Volume 276, September 2014, Pages 74-86, ISSN 0029-5493, http://dx.doi.org/10.1016/j.nucengdes.2014.05.022.

subjected different beams to air blast loading in a shock tube. The beams were made of reinforced concrete (some of which strengthened by fibers) and were simply supported. Considering the used amount of explosive and the distance of the beam from the charge, the load produced by the air blast can be considered as uniformly distributed (Magnusson et al., 2010). Further information on the characteristics of the beams and about the experimental apparatus is provided in Appendix A.1.

Two different beams tested by Magnusson and Hallgren (2000) are analyzed in this paper. The first one is labeled as "B40-D5" by the authors of the experiments. The time-history of the maximum transverse displacement v_{max}, registered at the mid-span section of the beam by a deflection gauge, is shown in grey line in Fig. 7. This curve has been interrupted at the instant of time when the maximum experimental concrete strain was recorded. This is in agreement with the failure criterion chosen in this paper, which is defined as the attainment of the maximum concrete strain.

The dashed black line of Fig. 7 represents the theoretical results given by the energy model. They are obtained by applying the Finite Difference scheme to Eq. (13), after substituting Eqs. (20), (21) and (22a) into it. Null initial conditions (i.e. V_0 (t=0) = dV_0/dt (t=0) = 0) are imposed, because the beam is at rest before the impulsive charge is detonated. The derivatives are approximated with finite differences of the 2nd order accuracy. Convergence studies have shown that a good choice of the time step is 10^{-5} s. The heavy dot inside the curve indicates the transition from the elastic to the plastic range, while the cross at the end of the curve identifies the maximum displacement, obtained when $\varepsilon_c = \varepsilon_{c,lim}$.

The prediction of the dynamic model is displayed in dotted black line in Fig. 7. This prediction is determined by solving the set of differential equations (29) through the Finite Difference method. The approximation of the derivatives with finite differences and the time step are identical to those adopted for the energy model. Initial displacement and velocity are set equal to zero also in this case.

Fig. 7 shows that the energy model gives a good estimation of the maximum displacement recorded experimentally, while the dynamic model provides a lower value than the experimental result.

Please cite this document as: F. Stochino, G. Carta, SDOF models for reinforced concrete beams under impulsive loads accounting for strain rate effects, Nuclear Engineering and Design, Volume 276, September 2014, Pages 74-86, ISSN 0029-5493, http://dx.doi.org/10.1016/j.nucengdes.2014.05.022.

Nonetheless, both the theoretical curves are very close to the experimental time-history.

It is important to notice that the last part of the experimental curve exhibits an abrupt change, which can be attributed either to a small damage of the experimental apparatus or, more probably, to the crushing of concrete.

The differences between the energy and the dynamic models are here explained. In the elastic regime, the maximum curvature determined with the energy model is $\theta = \pi^2/l^2 \cdot V_0$, while that computed through the dynamic model is given by Eq. (33a). Yielding is attained for a given value of the curvature. Therefore, since the coefficient that multiplies the displacement in the formula for the curvature of the energy model (i.e. π^2/l^2) is slightly larger than that of the dynamic model (i.e. $48/5l^2$), the yield displacement given by the energy model is slightly smaller than that calculated with the dynamic model. In the plastic regime, instead, the displacement obtained from the dynamic model is much smaller because the curvature is localized at the mid-span section due to the formation of a plastic hinge, hence the beam fails with a relatively small deflection. On the other hand, in the energy model the curvature is distributed along the whole beam (see Eq. (19)), hence the beam undergoes a larger displacement before reaching the ultimate limit state.

Please cite this document as: F. Stochino, G. Carta, SDOF models for reinforced concrete beams under impulsive loads accounting for strain rate effects, Nuclear Engineering and Design, Volume 276, September 2014, Pages 74-86, ISSN 0029-5493, http://dx.doi.org/10.1016/j.nucengdes.2014.05.022.

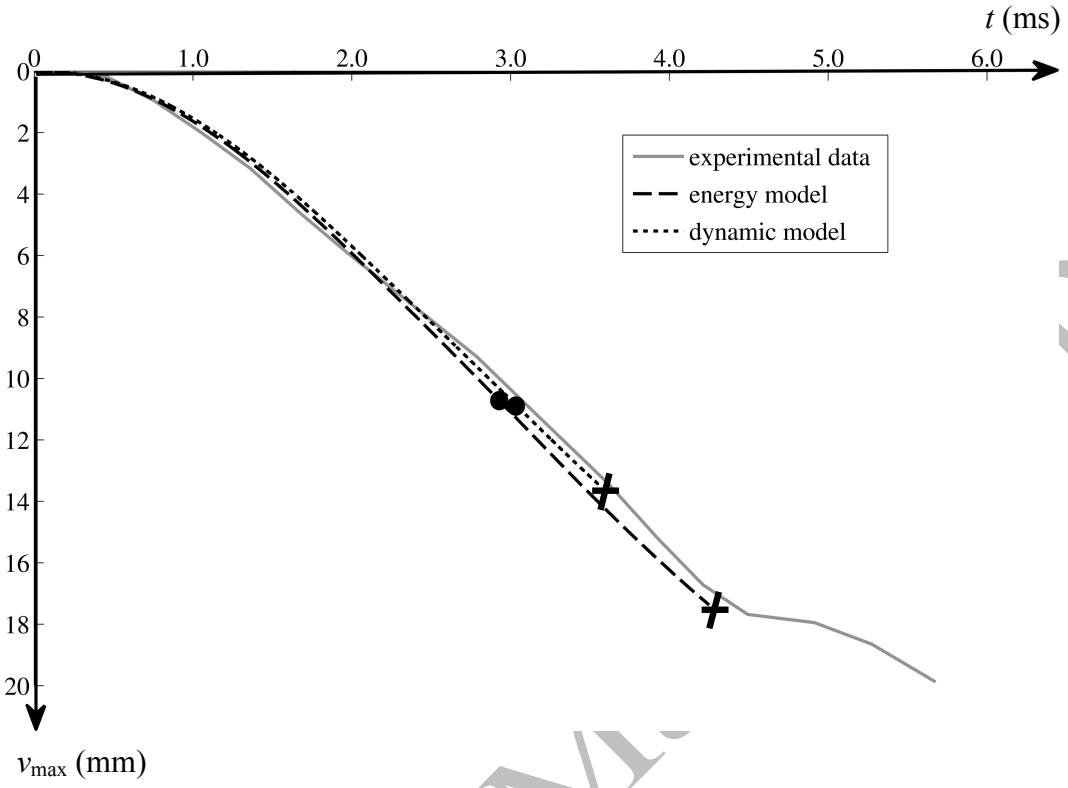

Fig. 7: Time-histories of the maximum deflection of beam B40-D5, tested by Magnusson and Hallgren (2000): experimental results (grey line); prediction given by the energy model (dashed black line); prediction provided by the dynamic model (dotted black line). For each model, the heavy dot represents the transition from the elastic to the plastic regime, while the cross indicates the attainment of the collapse criterion.

The results relative to another beam, denoted as "B100-D2(16)" by Magnusson and Hallgren (2000), are shown in Fig. 8. Similarly to beam B40-D5, the energy model provides an accurate prediction of the maximum displacement obtained experimentally, while the dynamic model underestimates it. We also observe that, in this case, there are some discrepancies between the theoretical and experimental time-histories, probably due to a non-uniform shock wave pressure on the beam (see Fig. A.3).

Please cite this document as: F. Stochino, G. Carta, SDOF models for reinforced concrete beams under impulsive loads accounting for strain rate effects, Nuclear Engineering and Design, Volume 276, September 2014, Pages 74-86, ISSN 0029-5493, http://dx.doi.org/10.1016/j.nucengdes.2014.05.022.

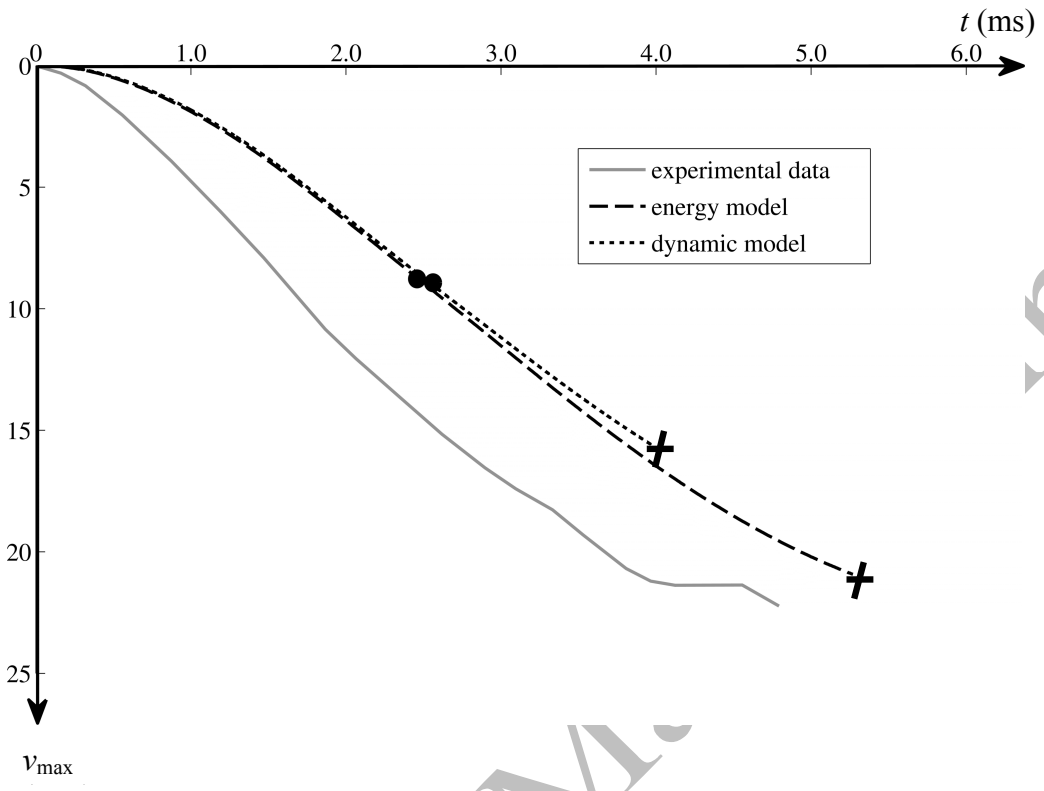

Fig. 8: Analogous curves to those displayed in Fig. 7, but relative to beam B100-D2(16), tested by Magnusson and Hallgren (2000).

5.2 RC beam under the impact of a drop hammer

In this section, a simply supported beam excited by a concentrated dynamic force acting at its mid-span section is examined. Such a force can be exerted by the drop of a weight, as in the experiments by Fujikake et al. (2009), who tested three different types of RC beams to the fall of a hammer from four different heights. Being under-reinforced, the beams exhibited a flexural failure. In this section, two beams belonging to the "S1616" series and subjected to the drop of the hammer from 1.2 m and 0.3 m are analyzed. The details of the tests are presented in Appendix A.2.

The experimental time-histories for these two cases are shown in grey lines in Figs. 9 and 10. The maximum concrete strains are not provided, therefore the curves have been cut off at the instant of time since the hammer stays in contact with the beam. In fact, at this instant of time the inertia of

Please cite this document as: F. Stochino, G. Carta, SDOF models for reinforced concrete beams under impulsive loads accounting for strain rate effects, Nuclear Engineering and Design, Volume 276, September 2014, Pages 74-86, ISSN 0029-5493, http://dx.doi.org/10.1016/j.nucengdes.2014.05.022.
the beam is increased by the additional mass of the hammer, which is not negligible because it is about three times larger than the mass of the beam. This instant of time can be easily identified from the time-history of the impact force, as it corresponds to the time when the force becomes almost constant (see Fujikake et al., 2009, Fig. 6).

The theoretical time-histories of the maximum displacements for the two beams under investigation, predicted by the energy model, are plotted in dashed black lines in Figs. 9 and 10. The theoretical values are calculated by employing the Finite Difference method to solve Eq. (13), where the kinetic energy, the strain energy and the external work are expressed by Eqs. (20), (21) and (22b), respectively. The dotted black lines in Figs. 9 and 10 represent, instead, the results of the dynamic model (Eqs. (29)). As in Section 5.1, for each case the separation between the elastic and plastic ranges and the fulfillment of the failure criterion are indicated by a heavy dot and a cross, respectively. It should be pointed out that, when the drop height is equal to 0.3 m (Fig. 10), the beam does not collapse, but the computations are stopped at the instant of time when the experimental curve has been truncated.

Please cite this document as: F. Stochino, G. Carta, SDOF models for reinforced concrete beams under impulsive loads accounting for strain rate effects, Nuclear Engineering and Design, Volume 276, September 2014, Pages 74-86, ISSN 0029-5493, http://dx.doi.org/10.1016/j.nucengdes.2014.05.022.

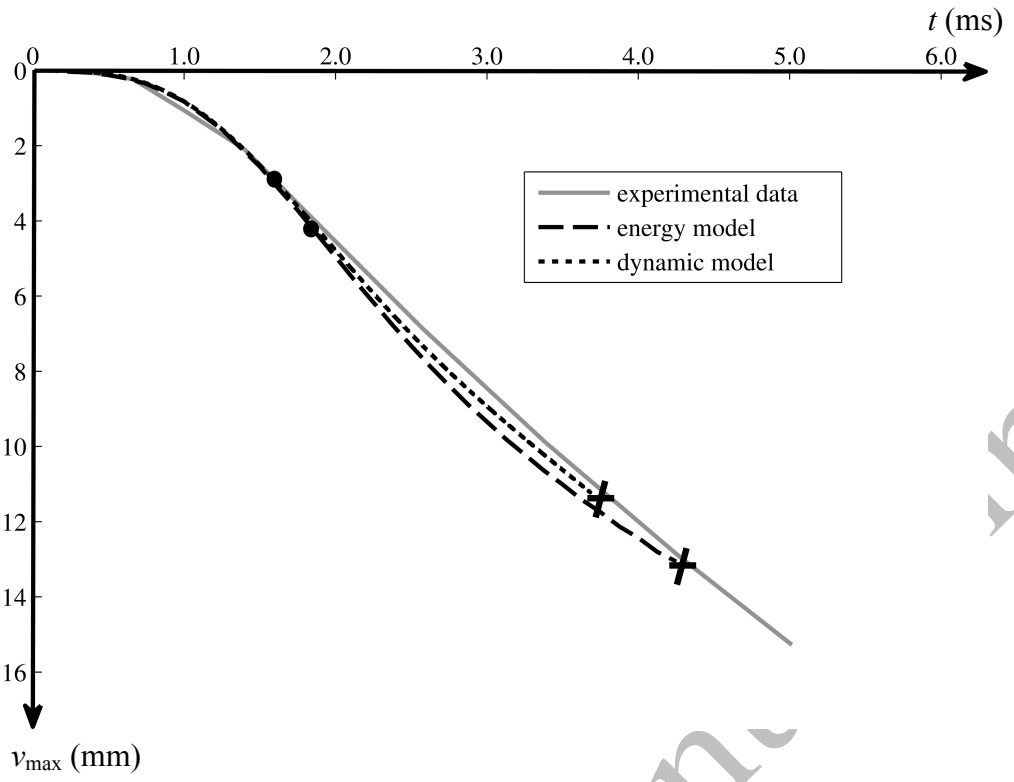

Fig. 9: Comparison between the experimental data taken from the paper by Fujikake et al. (2009) and the theoretical results obtained from the two models presented in this paper, relative to the beam of the S1616 series subjected to the drop of a hammer from a height of 1.2 m.

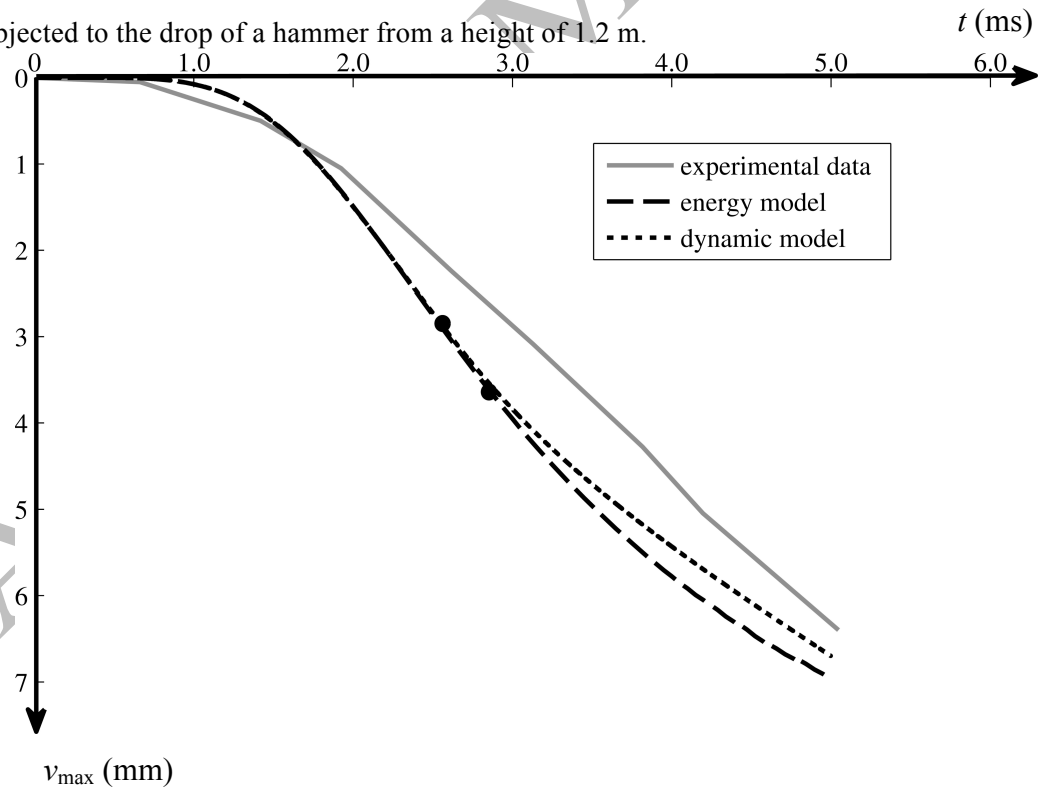

Fig. 10: Same as in Fig. 9, but in the case of a hammer falling from a height of 0.3 m.

Please cite this document as: F. Stochino, G. Carta, SDOF models for reinforced concrete beams under impulsive loads accounting for strain rate effects, Nuclear Engineering and Design, Volume 276, September 2014, Pages 74-86, ISSN 0029-5493, http://dx.doi.org/10.1016/j.nucengdes.2014.05.022.

In the case of the larger drop height, shown in Fig. 9, the energy model is the one which gives the best estimate of the maximum displacement. In addition, the theoretical curves are very close to the experimental findings. In the case of the smaller drop height, displayed in Fig. 10, the dynamic model provides a slightly better prediction of the test results.

In both Figs. 9 and 10, the yield displacement predicted by the energy model is larger that the yield displacement provided by the dynamic model. This is due to the fact that the yield curvature in the energy model is given by $\theta = \pi^2/l^2 \cdot V_0$, while the yield curvature in the dynamic model is calculated by means of Eq. (34a). Being $12 > \pi^2$, for the same value of the curvature that defines the yield state, the displacement at the end of the elastic regime produced by the dynamic model has to be smaller than the same displacement predicted by the energy model.

6. Strain rate effects

The theoretical curves shown in Figs. 7-10 were obtained by taking into account the variation of the material properties with strain rate. In this section, the same curves are determined by ignoring the influence of strain rate on the constitutive properties of concrete and reinforcing steel. This is accomplished by introducing the static properties of the materials into the formulations of the energy and dynamic models.

The time-histories of the deflections of the four beams investigated in Section 5, calculated without strain rate effects, are plotted in solid lines in Fig. 11. More specifically, Figs. 11a and 11b refer to the beams tested by Magnusson and Hallgren (2000), while Figs. 11c and 11d correspond to the experimental findings by Fujikake et al. (2009). In the same figures, the dashed lines are determined using the dynamic properties of the materials (these curves are identical to those displayed in Figs. 7-10). In addition, the percent differences between the two situations are included in Fig. 11 (the plus sign indicates that strain rate amplifies the maximum displacement, while the minus sign means that the maximum displacement is lower if strain rate effects are taken into account).

Please cite this document as: F. Stochino, G. Carta, SDOF models for reinforced concrete beams under impulsive loads accounting for strain rate effects, Nuclear Engineering and Design, Volume 276, September 2014, Pages 74-86, ISSN 0029-5493, http://dx.doi.org/10.1016/j.nucengdes.2014.05.022.

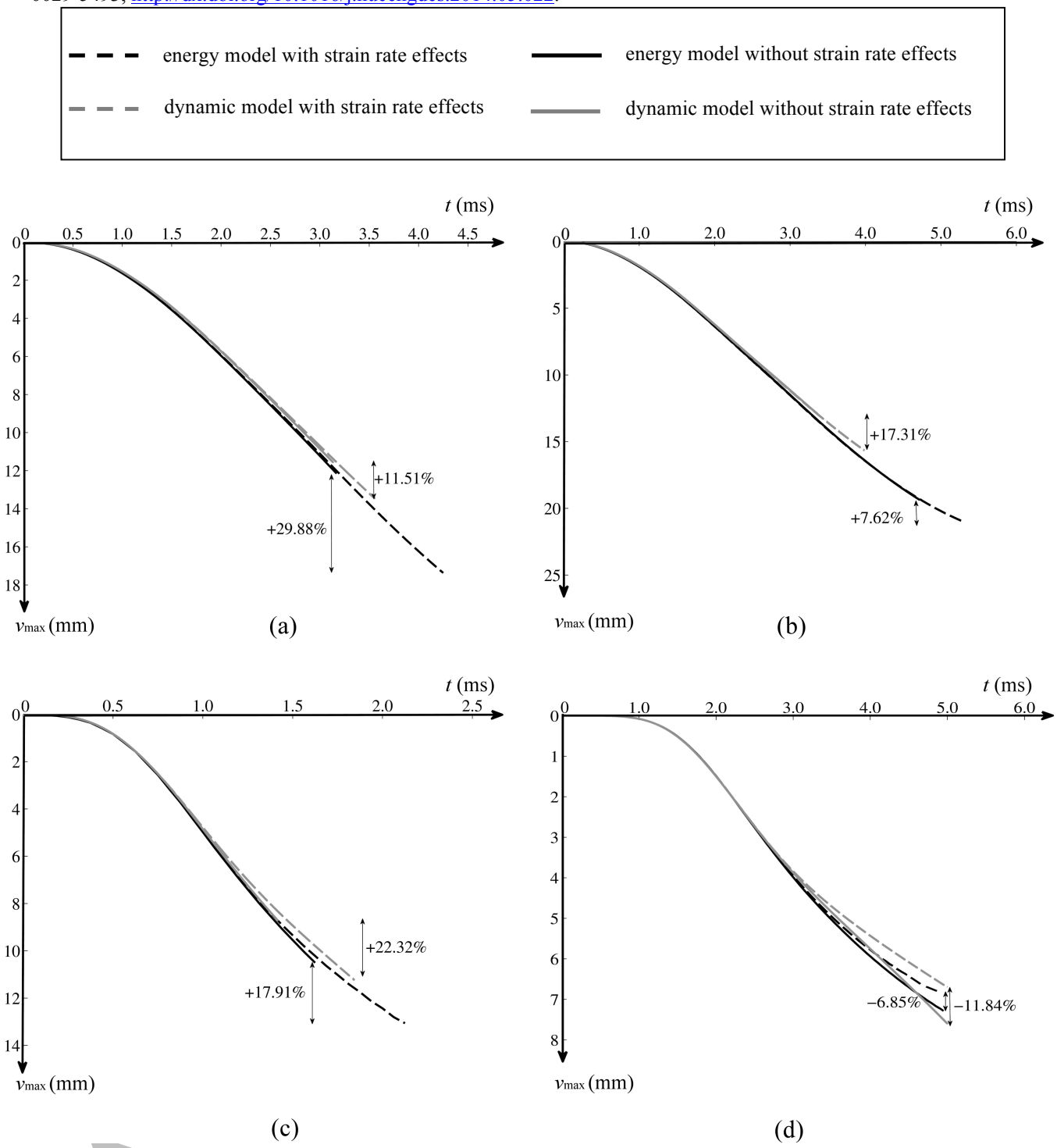

Fig. 11: Comparison between the deflection time-histories obtained without strain rate effects (solid lines) and with the influence of strain rate (dashed lines), for both the energy model (black lines) and the dynamic model (grey lines). Beams tested by Magnusson and Hallgren (2000): (a) B40-D5; (b) B100-D2(16). Beams tested by Fujikake et al. (2009): (c) S1616, drop height of 1.2 m; (d) S1616, drop height of 0.3 m.

From Fig. 11 it is apparent that, when the beam reaches the failure criterion (cases (a)-(c)), the

Please cite this document as: F. Stochino, G. Carta, SDOF models for reinforced concrete beams under impulsive loads accounting for strain rate effects, Nuclear Engineering and Design, Volume 276, September 2014, Pages 74-86, ISSN 0029-5493, http://dx.doi.org/10.1016/j.nucengdes.2014.05.022.

maximum displacement can be significantly increased by strain rate effects. This is due to the fact that the dynamic properties of the materials are larger than the static ones. Accordingly, also the characteristic properties of the section (i.e. M_y, M_u, θ_y, θ_u, $\bar{K}$, $\bar{M}$) are amplified. On the other hand, if the beam is far from failure (case (d)), the deflection of the beam is lower when dynamic properties are considered. This can be explained by comparing the bending moment - curvature diagrams with and without strain rate effects, which are displayed qualitatively in Fig. 12. This figure shows that the flexural stiffness of the beam is larger in the case with strain rate; therefore, if the beam is far from failure, namely for small values of the curvature, the maximum displacement detected in the beam at a certain time is lower if strain rate effects are taken into account. Nonetheless, the ultimate curvature in the case with strain rate is higher; accordingly, the beam undergoes a larger deflection before collapsing if strain rate effects are considered.

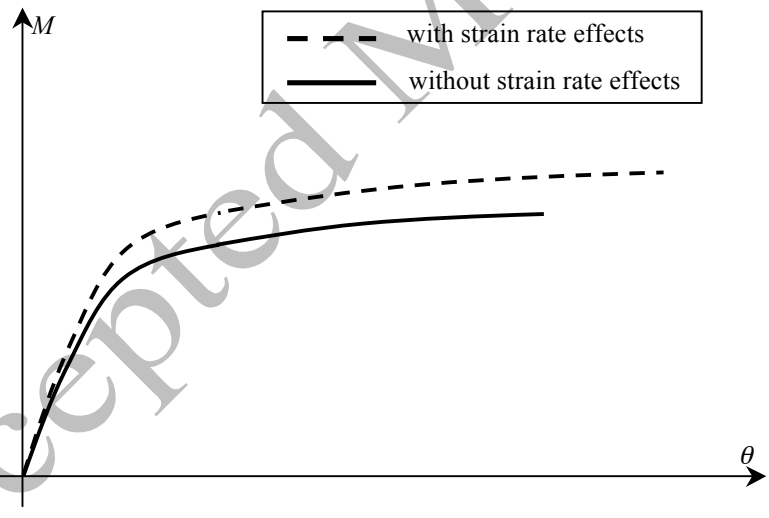

Fig. 12: Qualitative diagrams relating bending moment and curvature with and without strain rate effects.

Diagrams between bending moment and curvature similar to the curves sketched in Fig. 12 can be found in the paper by Asprone et al. (2012, Fig. 1), which show that both the maximum moment and the maximum curvature increase with the value of the strain rate.

Please cite this document as: F. Stochino, G. Carta, SDOF models for reinforced concrete beams under impulsive loads accounting for strain rate effects, Nuclear Engineering and Design, Volume 276, September 2014, Pages 74-86, ISSN 0029-5493, http://dx.doi.org/10.1016/j.nucengdes.2014.05.022.

7. Conclusions

In this paper, two models characterized by one degree of freedom have been proposed to calculate the response of a structural element under impulsive loads: the energy model, based on the law of energy balance, and the dynamic model, developed from the equation of motion of a forced mass-spring oscillator. Both models are simple and easy to implement in numerical codes. Furthermore, since there is only one unknown to determine, the computational time required to obtain the solution of the problem is very short. For all these reasons, both models are convenient to use in practical applications.

Under impulsive loads (explosions, high impacts, etc.), the strain rates of the materials of the RC beam result to be very large. Therefore, strain rate effects have been incorporated into the formulations of the two models by modifying the constitutive properties of concrete and reinforcing steel in each time step of the computational process. The importance of accounting for strain rate effects has been demonstrated explicitly in this paper by showing that the results obtained with strain rate effects are very different from those derived with the static properties of the materials. Comparison with test data relative to different experiments found in literature has shown that the energy model provides a good prediction of the maximum displacement of the structural element at failure, while the dynamic model generally underestimates it. In addition, in most of the cases examined, the time-history of the maximum deflection determined with either of the two models is close to the experimental time-history. However, it should be remarked that both models are based on some approximations. In particular, in the energy model it is assumed that the shape of the structural element coincides with its first vibration mode. In the dynamic model, instead, the equivalent parameters of the oscillator (mass, stiffness and load) and the length of the plastic hinge are estimated by means of approximate formulae.

In future work, it is intended to include more vibration modes (and, hence, more degrees of freedom) in the formulation of the energy model, in order to check if the theoretical results are improved. In addition, structural elements with different boundary conditions and applied loads will

Please cite this document as: F. Stochino, G. Carta, SDOF models for reinforced concrete beams under impulsive loads accounting for strain rate effects, Nuclear Engineering and Design, Volume 276, September 2014, Pages 74-86, ISSN 0029-5493, http://dx.doi.org/10.1016/j.nucengdes.2014.05.022.
be investigated.

An alternative approach to study the dynamic response of a beam under impulsive loads consists in employing the Finite Element Method (FEM). This method should be formulated such that the variations of the material properties with strain rate are taken into account, otherwise the numerical results would not fit well the experimental data (Carta and Stochino, 2013). The FEM is a consolidated, versatile and powerful tool, that is suitable to solve complex problems. On the other hand, the models presented in this paper are simpler and need less input parameters, hence they can be useful to better understand the physics underneath the problem. Moreover, they demand far less computational effort, thus they can be used to process large sets of data in a reasonable time, as required for example in sensitivity analyses.

Acknowledgements

The authors would like to thank the Swedish Defence Research Agency (FOI) for having provided the reports by Magnusson and Hallgren (2000, 2003).

Appendix A. Experimental details

In this appendix, detailed information on the experimental tests considered in this paper is presented.

A.1 Tests by Magnusson and Hallgren (2000)

Magnusson and Hallgren (2000) subjected simply supported RC beams to the pressure waves generated by the detonations of sphere-shape explosive charges. The experiments were conducted in a shock tube, schematized in Fig. A.1. The beams had a doubly reinforced rectangular cross-section, and stirrups were provided to increase the shear strength. The geometrical and mechanical properties of the beams analyzed in this paper are reported in Table A.1.

Please cite this document as: F. Stochino, G. Carta, SDOF models for reinforced concrete beams under impulsive loads accounting for strain rate effects, Nuclear Engineering and Design, Volume 276, September 2014, Pages 74-86, ISSN 0029-5493, http://dx.doi.org/10.1016/j.nucengdes.2014.05.022.

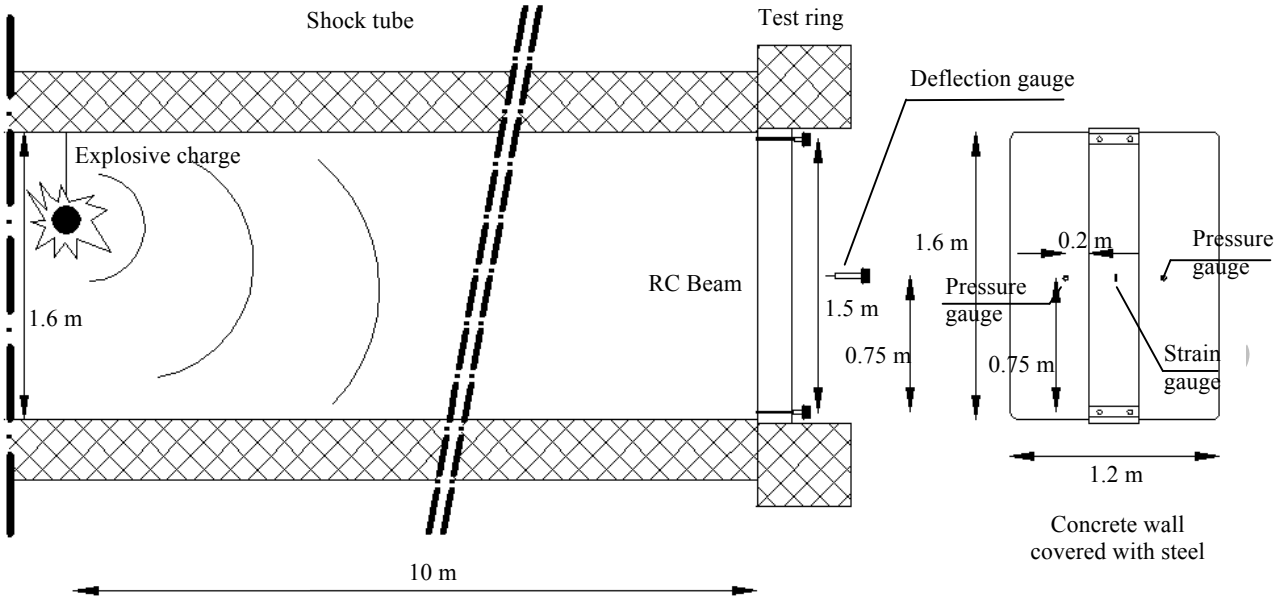

Fig. A.1: Experimental setup of the tests performed by Magnusson and Hallgren (2000).

	B40-D5	B100-D2(16)
span of the beam	1.5 m	1.5 m
width of the cross-section	0.300 m	0.300 m
depth of the cross-section	0.160 m	0.160 m
cover	0.025 m	0.025 m
tensile reinforcement	5 ϕ16 mm	5 ϕ16 mm
compressive reinforcement	2 ϕ10 mm	2 ϕ10 mm
compressive strength of concrete	43 MPa	109 MPa
yield strength of reinforcing steel	604 MPa	604 MPa
Young's modulus of reinforcing steel	210 GPa	210 GPa

Table A.1: Characteristics of the beams tested by Magnusson and Hallgren (2000).

The pressures registered on the two beams are shown in Figs. A.2 and A.3. In each figure two

Please cite this document as: F. Stochino, G. Carta, SDOF models for reinforced concrete beams under impulsive loads accounting for strain rate effects, Nuclear Engineering and Design, Volume 276, September 2014, Pages 74-86, ISSN 0029-5493, http://dx.doi.org/10.1016/j.nucengdes.2014.05.022.

diagrams are plotted, because two pressure gauges were employed by Magnusson and Hallgren for each beam. In the numerical computations, the average of the two diagrams has been used to calculate the dynamic load acting on each beam. It is worth noticing that the time-history of the load is very irregular and jagged, hence a closed form solution of the problem cannot be obtained.

In Tables A.2 and A.3, the maximum concrete strains in the two beams registered in the experiments are compared with the corresponding quantities obtained from the two models. In the same tables, the theoretical strain rates of both tensile and compressive reinforcements are indicated. Yielding is reached only in the tensile reinforcing steels.

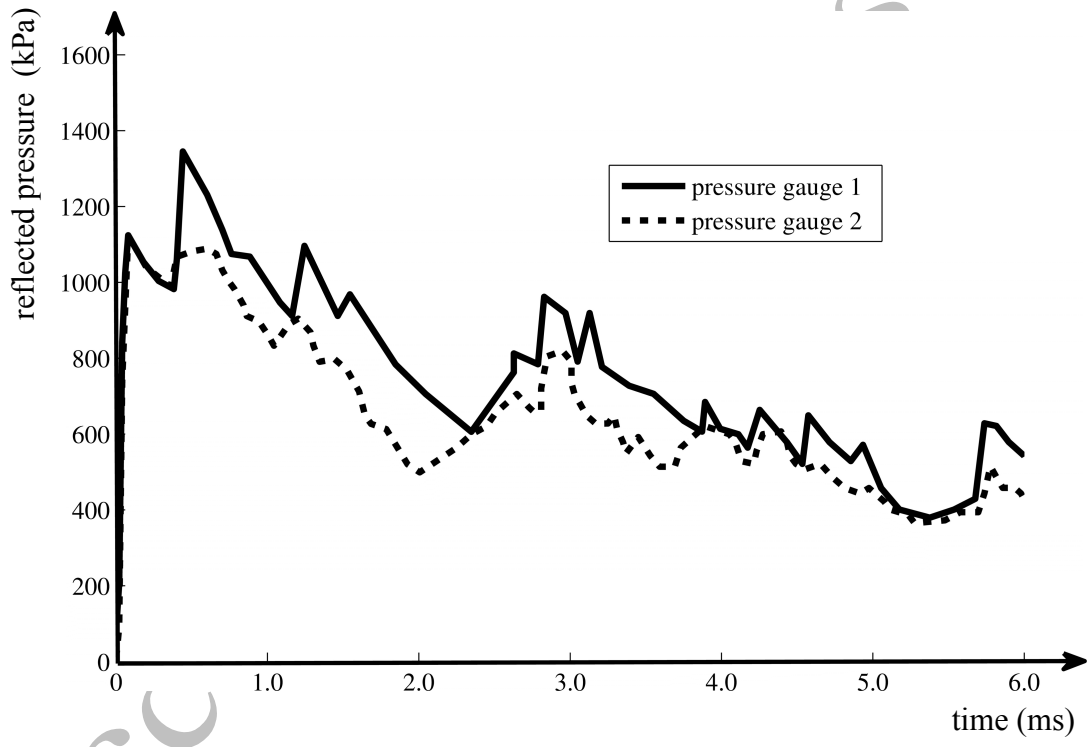

Fig. A.2: Reflected pressures recorded on beam B40-D5 (Magnusson and Hallgren, 2000, Fig. A1.6).

Please cite this document as: F. Stochino, G. Carta, SDOF models for reinforced concrete beams under impulsive loads accounting for strain rate effects, Nuclear Engineering and Design, Volume 276, September 2014, Pages 74-86, ISSN 0029-5493, http://dx.doi.org/10.1016/j.nucengdes.2014.05.022.

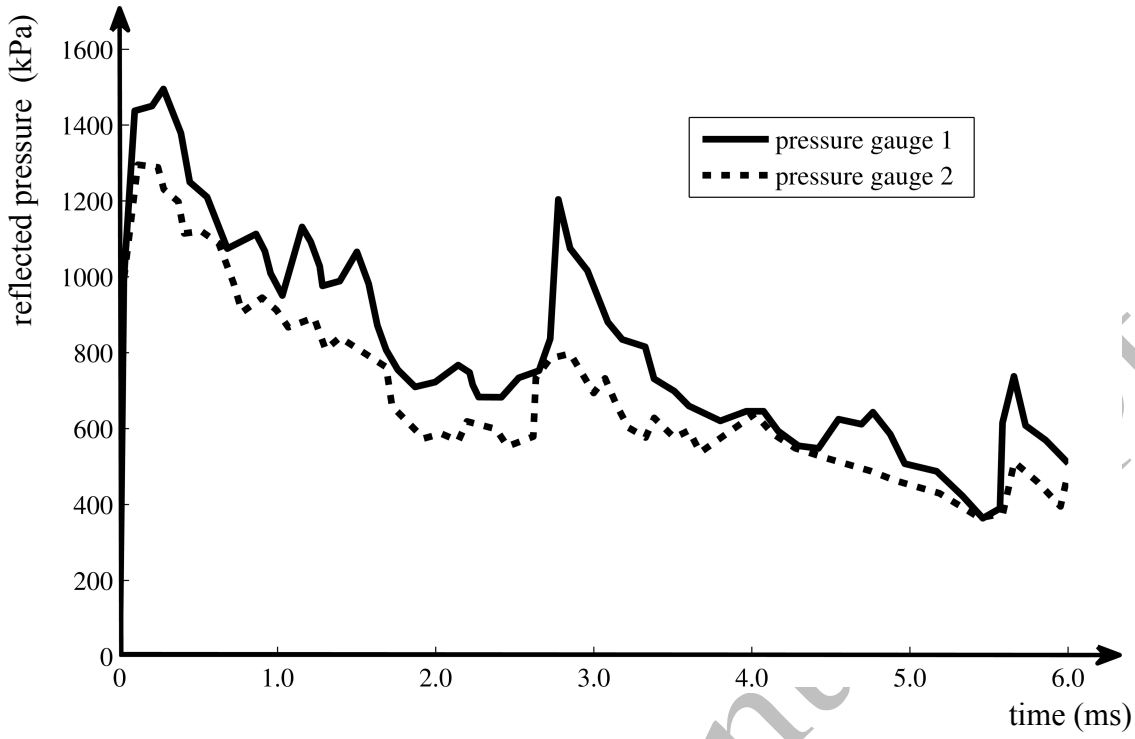

Fig. A.3: Reflected pressures recorded on beam B100-D2(16) (Magnusson and Hallgren, 2000, Fig. A1.8).

	$\varepsilon_{c,lim}$ (‰)	ε_s (‰)	ε_{ss} (‰)
experimental values	3.6	---	---
energy model	4.3	5.3	2.0
dynamic model	4.4	5.7	2.0

Table A.2: Strains relative to beam B40-D5.

	$\varepsilon_{c,lim}$ (‰)	ε_s (‰)	ε_{ss} (‰)
experimental values	5.0	---	---
energy model	3.7	9.6	0.6
dynamic model	3.7	10.6	0.4

Table A.3: Strains relative to beam B100-D2(16).

Please cite this document as: F. Stochino, G. Carta, SDOF models for reinforced concrete beams under impulsive loads accounting for strain rate effects, Nuclear Engineering and Design, Volume 276, September 2014, Pages 74-86, ISSN 0029-5493, http://dx.doi.org/10.1016/j.nucengdes.2014.05.022.

A.2 Tests by Fujikake et al. (2009)

Fujikake and co-workers carried out impact load tests with the experimental apparatus sketched in Fig. A.4. The hammer was dropped from different heights. In this paper, we have considered the S1616 series of beams, and in particular the results obtained with a drop height of 1.2 m and with a drop height of 0.3 m.

Also in this case, the beams were simply supported, had a doubly reinforced rectangular cross-section and contained stirrups. The details of the beams belonging to the S1616 series are provided in Table A.4.

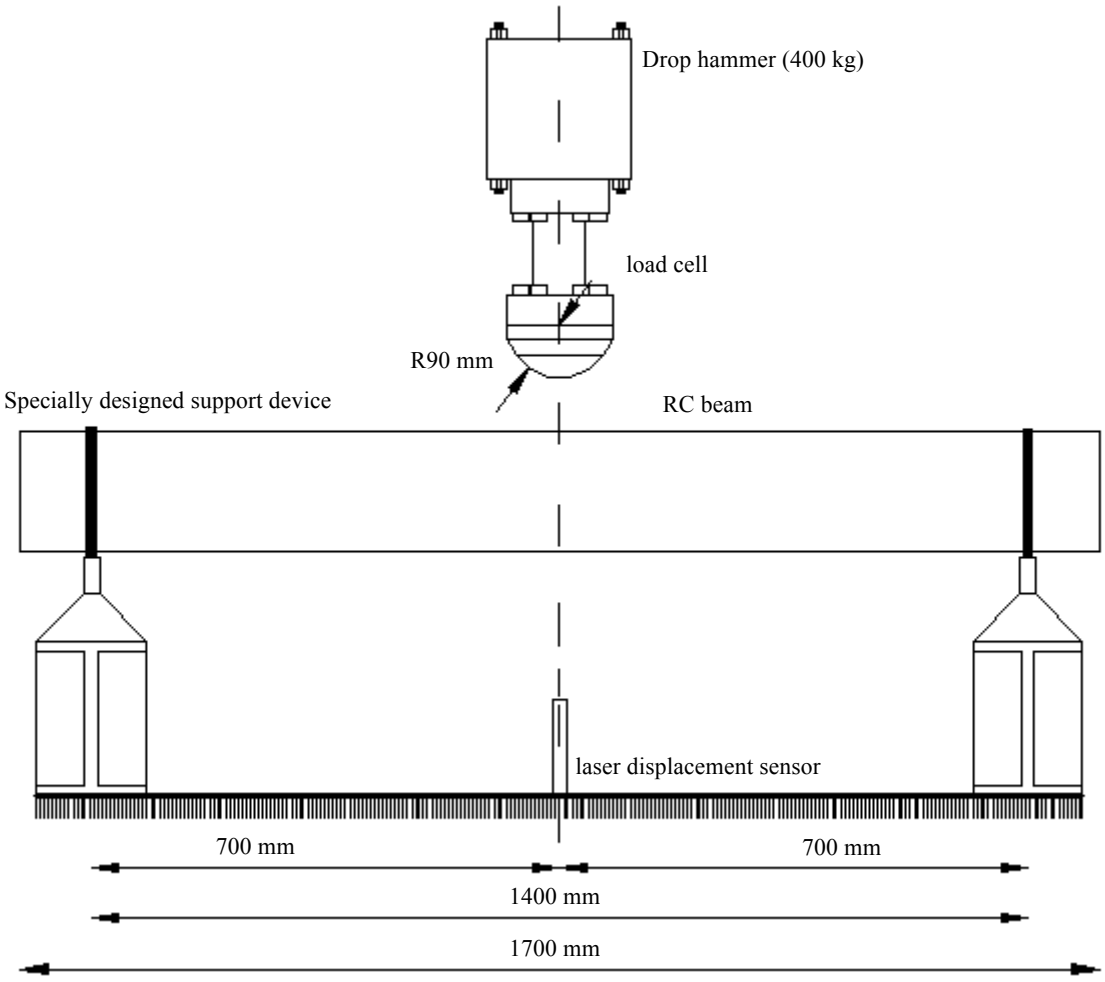

. A.4: Experimental setup designed by Fujikake et al. (2009).

Please cite this document as: F. Stochino, G. Carta, SDOF models for reinforced concrete beams under impulsive loads accounting for strain rate effects, Nuclear Engineering and Design, Volume 276, September 2014, Pages 74-86, ISSN 0029-5493, http://dx.doi.org/10.1016/j.nucengdes.2014.05.022.

span of the beam	1.4 m
width of the cross-section	0.15 m
depth of the cross-section	0.25 m
cover	0.04 m
area of tensile reinforcement	$3.97 \cdot 10^{-4}$ m^2
area of compressive reinforcement	$3.97 \cdot 10^{-4}$ m^2
compressive strength of concrete	42 MPa
yield strength of reinforcing steel	426 MPa

Table A.4: Geometrical and mechanical properties of the S1616 series of beams tested by Fujikake et al. (2009).

The contact force between the hammer and the beam was recorded during time by using a load cell. The time-histories of the contact forces for the S1616 series with 1.2 m drop height and with 0.3 m drop height are shown in Fig. A.5 and Fig. A.6, respectively.

Unfortunately, Fujikake and co-authors did not measure the strains of concrete and reinforcing steels.

Please cite this document as: F. Stochino, G. Carta, SDOF models for reinforced concrete beams under impulsive loads accounting for strain rate effects, Nuclear Engineering and Design, Volume 276, September 2014, Pages 74-86, ISSN 0029-5493, http://dx.doi.org/10.1016/j.nucengdes.2014.05.022.

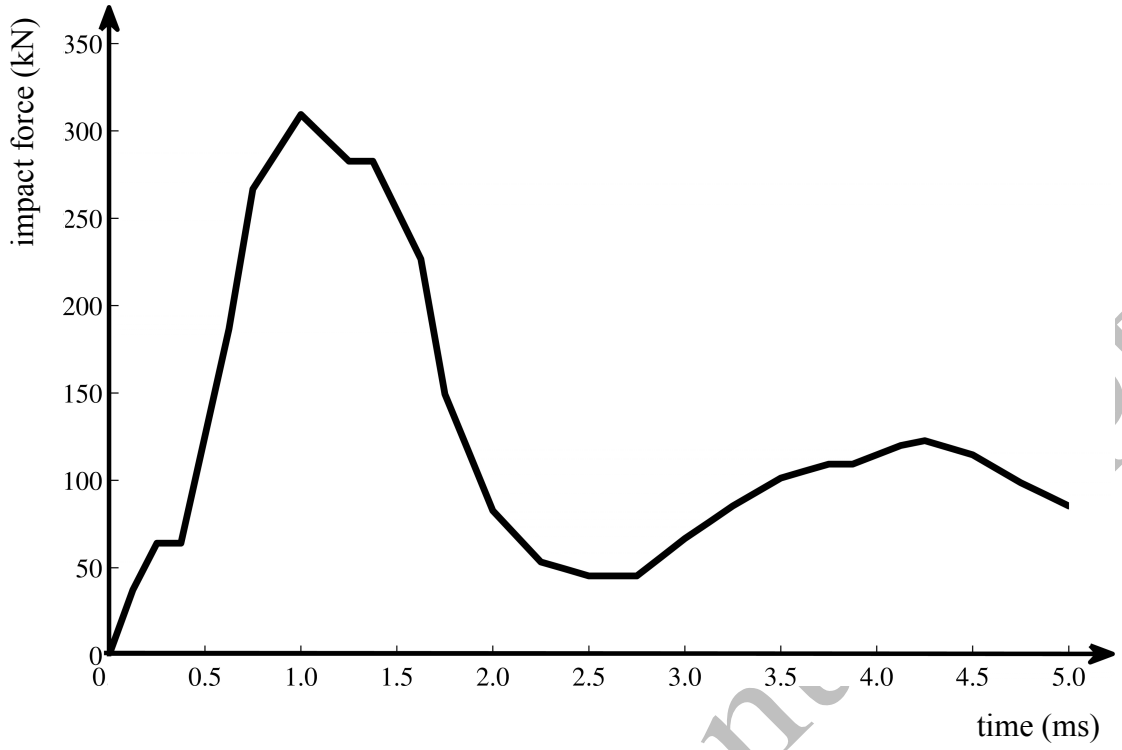

Fig. A.5: Impact force versus time for the S1616 series of beams, with a drop height equal to 1.2 m (Fujikake et al. (2009), Fig. 5d).

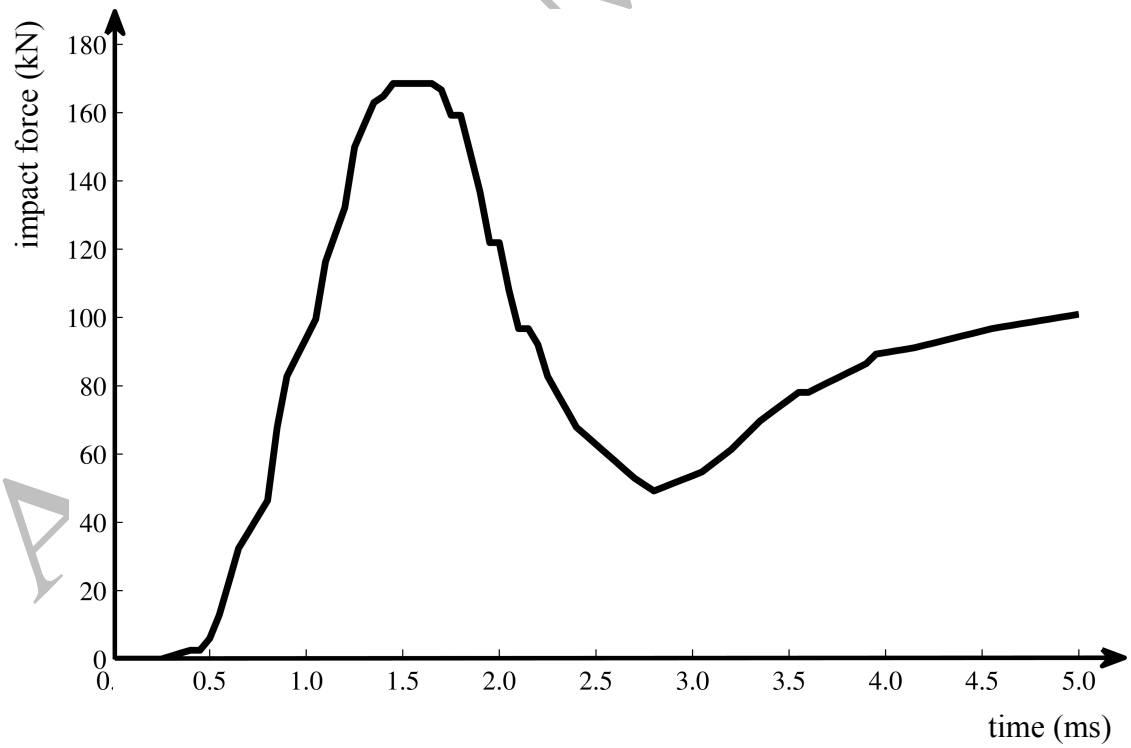

Fig. A.6: Impact force versus time for the S1616 series of beams, with a drop height equal to 0.3 m (Fujikake et al. (2009), Fig. 5b).

Please cite this document as: F. Stochino, G. Carta, SDOF models for reinforced concrete beams under impulsive loads accounting for strain rate effects, Nuclear Engineering and Design, Volume 276, September 2014, Pages 74-86, ISSN 0029-5493, http://dx.doi.org/10.1016/j.nucengdes.2014.05.022.

References

Alves, M., Jones, N., 2002. Impact failure of beams using damage mechanics: Part II – Application. Int. J. Impact Eng. 27, 863-890.

Asprone, D., Frascadore, R., Di Ludovico, M., Prota, A., Manfredi, G., 2012. Influence of strain rate on the seismic response of RC structures. Eng. Struct. 35, 29-36.

Biggs, J.M., 1964. Introduction to structural dynamics. McGraw-Hill Book Company, New York.

Carta, G., Stochino, F., 2013. Theoretical models to predict the flexural failure of reinforced concrete beams under blast loads. Eng. Struct. 49, 306-315.

Comité Euro-International du Béton, 1988. Concrete structures under impact and impulsive loading, CEB Bulletin n. 187. Lausanne, Switzerland.

Cox, P.A., Westine, P.S., Kulesz, J.J., Esparza, E.D., 1978. Analysis and evaluation of suppressive shields, Report ARCSL-CR-77028 n.10. Southwest Research Institute, San Antonio, Texas.

Crupi, V., Epasto, G., Guglielmino, E., 2012. Collapse modes in aluminium honeycomb sandwich panels under bending and impact loading. Int. J. Impact Eng. 43, 6-15.

Fischer, K., Häring, I., 2009. SDOF response model parameters from dynamic blast loading experiments. Eng. Struct. 31, 1677-1686.

Foo, C.C., Seah, L.K., Chai, G.B., 2011. A modified energy-balance model to predict low-velocity impact response for sandwich composites. Comp. Struct. 93, 1385-1393.

Fujikake, K., Li, B., Soeun, S., 2009. Impact response of reinforced concrete beam and its analytical evaluation. J. Struct. Eng. ASCE 135, 938-950.

Hudson, J.L., Darwin, D., 2005. Evaluation and repair of blast damaged reinforced concrete buildings, SL report 05-1. University of Kansas Center for Research, Inc., Lawrence, Kansas.

International Federation for Structural Concrete, 2010. Model Code 2010, First Complete Draft, Vol. 1, fib Bulletin n. 55. Lausanne, Switzerland.

Kusano, N., Aoyagi, J., Aizana, J., 1992. Impulsive local damage analysis of concrete structure by

the distinct element method. Nucl. Eng. Des. 138, 105-110.

Li, B., Pan, T.C., Nair, A., 2009. A case study of the effect of cladding panels on the response of reinforced concrete frames subjected to distant blast loadings. Nucl. Eng. Des. 239, 455-469.

Magnusson, J., Hallgren, M., 2000. High performance concrete beams subjected to shock waves from air blast, Report n. FOA-R-00-01586-311-SE. Defence Research Establishment (FOA), Tumba, Sweden.

Magnusson, J., Hallgren, M., 2003. High performance concrete beams subjected to shock waves from air blast, Part 2, Report n. FOI-R-1116-SE. Swedish Defence Research Agency (FOI), Tumba, Sweden.

Magnusson, J., Hallgren, M., Ansell, A., 2010. Air-blast-loaded, high-strength concrete beams. Part I: Experimental investigation. Mag. Concr. Res. 62, 127-136.

Masuya, H., Kajikana, Y., Nakata, Y., 1994. Application of the distinct element method to the analysis of the concrete members under impact. Nucl. Eng. Des. 150, 367-377.

Morison, C.M., 2006. Dynamic response of walls and slabs by single-degree-of-freedom analysis—a critical review and revision. Int. J. Impact Eng. 32, 1214-1247.

Nassr, A.A., Razaqpur, A.G., Tait, M.J., Campidelli, M., Foo, S., 2012. Single and multi degree of freedom analysis of steel beams under blast loading. Nucl. Eng. Des. 242, 63-77.

Nassr, A.A., Razaqpur, A.G., Tait, M.J., Campidelli, M., Foo, S., 2013. Strength and stability of steel beam columns under blast load. Int. J. Impact Eng. 55, 34-48.

Riedel, W., Fischer, K., Kranzer, C., Erskine, J., Cleave, R., Hadden, D., Romani, M., 2012. Modeling and validation of wall-window retrofit system under blast loading. Eng. Struct. 37, 235-245.

Tachibana, S., Masuya, H., Nakamura, S., 2010. Performance based design of reinforced concrete beams under impact. Nat. Hazards Earth. Syst. Sci. 10, 1069-1078.

Westine, P.S., Baker, W.E., 1975. Energy solutions for predicting deformation in blast-loaded structures, Report EM-CR-76027 n.6. Southwest Research Institute, San Antonio, Texas.

Please cite this document as: F. Stochino, G. Carta, SDOF models for reinforced concrete beams under impulsive loads accounting for strain rate effects, Nuclear Engineering and Design, Volume 276, September 2014, Pages 74-86, ISSN 0029-5493, http://dx.doi.org/10.1016/j.nucengdes.2014.05.022.
Yang, G., Lok, T.-S., 2007. Analysis of RC structures subjected to air-blast loading accounting for strain rate effect of steel reinforcement. Int. J. Impact Eng. 34, 1924-1935.

Please cite this document as: F. Stochino, G. Carta, SDOF models for reinforced concrete beams under impulsive loads accounting for strain rate effects, Nuclear Engineering and Design, Volume 276, September 2014, Pages 74-86, ISSN 0029-5493, http://dx.doi.org/10.1016/j.nucengdes.2014.05.022.

List of figures captions

Fig. 1: Relations between stress and strain for concrete (a) and reinforcing steel (b) considered in this paper.

Fig. 2: (a) Cross-section of a doubly reinforced concrete beam. Yield state: stress diagram (b) and strain diagram (c). Ultimate state: stress diagram (d) and strain diagram (e).

Fig. 3: (a) Bilinear relation between bending moment and curvature; (b) smooth bending moment - curvature relation considered in this work, obtained from Eq. (10).

Fig. 4: Schematic representation of the beam, subjected to a distributed load q, to point forces F_i and to concentrated moments M_j.

Fig. 5: (a) Equivalent SDOF oscillator representing the beam of Fig. 4, having mass M_E and stiffness K_E; the displacement generated by the force P_E is indicated by v_E. (b) Load-displacement diagram of the equivalent SDOF oscillator.

Fig. 6: (a) Assumed deformation mechanism in the plastic range, with the generation of a plastic hinge at the mid-span section of the beam; (b) detail of the plastic hinge.

Fig. 7: Time-histories of the maximum deflection of beam B40-D5, tested by Magnusson and Hallgren (2000): experimental results (grey line); prediction given by the energy model (dashed black line); prediction provided by the dynamic model (dotted black line). For each model, the heavy dot represents the transition from the elastic to the plastic regime, while the cross indicates the attainment of the collapse criterion.

Fig. 8: Analogous curves to those displayed in Fig. 7, but relative to beam B100-D2(16), tested by Magnusson and Hallgren (2000).

Fig. 9: Comparison between the experimental data taken from the paper by Fujikake et al. (2009) and the theoretical results obtained from the two models presented in this paper, relative to the beam of the S1616 series subjected to the drop of a hammer from a height of 1.2 m.

Fig. 10: Same as in Fig. 9, but in the case of a hammer falling from a height of 0.3 m.

Fig. 11: Comparison between the deflection time-histories obtained without strain rate effects (solid lines) and with the influence of strain rate (dashed lines), for both the energy model (black lines) and the dynamic model (grey lines). Beams tested by Magnusson and Hallgren (2000): (a) B40-D5; (b) B100-D2(16). Beams tested by Fujikake et al. (2009): (c) S1616, drop height of 1.2 m; (d) S1616, drop height of 0.3 m.

Fig. 12: Qualitative diagrams relating bending moment and curvature with and without strain rate effects.

Please cite this document as: F. Stochino, G. Carta, SDOF models for reinforced concrete beams under impulsive loads accounting for strain rate effects, Nuclear Engineering and Design, Volume 276, September 2014, Pages 74-86, ISSN 0029-5493, http://dx.doi.org/10.1016/j.nucengdes.2014.05.022.

Fig. A.1: Experimental setup of the tests performed by Magnusson and Hallgren (2000).

Fig. A.2: Reflected pressures recorded on beam B40-D5 (Magnusson and Hallgren, 2000, Fig. A1.6).

Fig. A.3: Reflected pressures recorded on beam B100-D2(16) (Magnusson and Hallgren, 2000, Fig. A1.8).

Fig. A.4: Experimental setup designed by Fujikake et al. (2009).

Fig. A.5: Impact force versus time for the S1616 series of beams, with a drop height equal to 1.2 m (Fujikake, 2009, Fig. 5d).

Fig. A.6: Impact force versus time for the S1616 series of beams, with a drop height equal to 0.3 m (Fujikake, 2009, Fig. 5b).

List of tables captions

Table A.1: Characteristics of the beams tested by Magnusson and Hallgren (2000).

Table A.2: Strains relative to beam B40-D5.

Table A.3: Strains relative to beam B100-D2(16).

Table A.4: Geometrical and mechanical properties of the S1616 series of beams tested by Fujikake et al. (2009).